CORRELATION ANALYSIS OF OPTIMAL ORIENTATION AND TILTING OF PV ARRAY USING VARIOUS TYPES OF SOLAR DATABASE

KOH YONG SER

A project report submitted in partial fulfilment of the requirements for the award of Bachelor of Science Physics with Honours

Lee Kong Chian Faculty of Engineering and Science
Universiti Tunku Abdul Rahman

May 2024

DECLARATION

I hereby declare that this project report is based on my original work except for citations and quotations which have been duly acknowledged. I also declare that it has not been previously and concurrently submitted for any other degree or award at UTAR or other institutions.

Signature : KOH YONG SER

Name : Koh Yong Ser

ID No. : 2200837

Date : 18th September 2024

APPROVAL FOR SUBMISSION

I certify that this project report entitled **"CORRELATION ANALYSIS OF OPTIMAL ORIENTATION AND TILTING OF PV ARRAY USING VARIOUS TYPES OF SOLAR DATABASE"** was prepared by **KOH YONG SER** has met the required standard for submission in partial fulfilment of the requirements for the award of Bachelor of Science Physics with Honours at Universiti Tunku Abdul Rahman.

Approved by,

Signature	:	
Supervisor	:	Dr. Lim Boon Han
Date	:	18 September 2024
Signature	:	
Co-Supervisor	:	
Date	:	

ACKNOWLEDGEMENTS

I would like to express my heartfelt gratitude to everyone who has contributed to the successful completion of this project. First and foremost, I am deeply thankful to my project supervisor, Ir. Dr. Lim Boon Han, for his unwavering guidance, professional expertise, and patience throughout the entire research process. His insights, especially in the field of solar energy and the technical aspects of my analysis, were invaluable and significantly contributed to the progress and success of this project.

I would also like to sincerely thank Universiti Tunku Abdul Rahman (UTAR) for providing access to essential resources, including the online library and research facilities. The availability of these resources greatly facilitated my research and enabled me to gather the necessary information efficiently.

A special thank you goes to my loving parents, whose unwavering financial and emotional support created a conducive environment for me to focus on my work. Their encouragement and belief in my abilities helped me overcome challenges along the way, and I am deeply grateful for their constant presence throughout this journey.

Lastly, to my friends and everyone else who has supported me during this time, your encouragement and assistance have not gone unnoticed. Thank you all for your contributions, without which the completion of this project would not have been possible.

ABSTRACT

This project investigates the optimal tilt angle and orientation for photovoltaic (PV) systems in tropical regions. Recognizing the limitations of previous research, this study expands the scope by considering a broader range of locations, orientations, and interrow spacing (DL ratio) while incorporating the Perez sky model to accurately account for diffuse radiation components. The research utilizes simulated data from both SolarGIS and PVGIS databases, employing Typical Meteorological Year (TMY) and Time Series (TS) data types to determine optimal parameters that maximize global tilted irradiance (GTI). The analysis reveals that the results from both TMY and TS data are close enough to suggest their universality, allowing for the use of TMY data to significantly reduce simulation time without sacrificing accuracy, as TMY provides representative weather data. Optimal tilt angles generally increase with latitude, aligning with theoretical expectations but deviating at lower latitudes, likely due to the influence of tropical climate factors. Optimal orientation shows a distinct shift from south to southeast and east as latitude decreases, challenging the conventional assumption that south-facing panels are universally ideal. Further analysis establishes a DL ratio of 1.5 as ideal for achieving consistent performance, balancing interrow shading with efficient land usage. Interestingly, the study demonstrates that minor variations in tilt angle (±3°) and orientation (±30°) have a negligible impact on energy production, providing flexibility during installation. Additionally, the simulation's accuracy is validated through comparison with experimental data collected from a PV system in Malaysia. The experimental results, while limited in scope due to practical constraints, align with the simulated predictions, particularly regarding optimal orientation. This research provides insights for PV system designers and installers in tropical regions, emphasizing the significance of latitude-specific adjustments and interrow spacing optimization. The findings contribute to a deeper understanding of the interplay between geographical factors and PV system configurations for maximizing energy yield in tropical climates.

TABLE OF CONTENTS

LIST OF TABLES

LIST OF FIGURES

LIST OF SYMBOLS / ABBREVIATIONS

I_T	total incident solar radiation, W/m^2
I_B	direct component of the solar radiation, W/m^2
I_D	diffuse component of the solar radiation, W/m^2
I_R	reflected component of the solar radiation, W/m^2
I_0	extraterrestrial radiation, W/m^2
R_b	coefficient of the direct component of the solar radiation
R_d	coefficient of the diffuse component of the solar radiation
R_r	coefficient of the reflected component of the solar radiation
F_1	circumsolar coefficients
F_2	horizon brightness coefficients
f_{ij}	coefficients of the Perez model
m	air mass
f_s	shade factor
d	interrow spacing distance between the PV arrays, m
l	length of the solar panel, m
I	solar cell output current, A
I_{ph}	light generated current, A
V	voltage across the cell terminals, V
T	operating temperature of the solar cell, K
e	electron charge, 1.602×10^{-19} C
k_B	Boltzmann constant, 1.381×10^{-23} J/K
n	ideality factor
t_m	operating temperature of the solar, ℃
t_a	ambient temperature, ℃
k_{Ross}	Ross coefficient, ℃m^2/W
P_{mp2}	PV maximum output power after considering temperature effect, W
P_{mp1}	PV maximum output power before considering temperature effect, W
f_{temp}	temperature factor

$\vec{I}$	solar radiation vector
$\vec{N}$	normal vector of the PV module surface
ρ	ground Aledo
θ_z	solar zenith angle, °
α	solar altitude angle, $\alpha = 90° - \theta_z$, °
ω	hour angle, in the local solar time, °
δ	current declination of the Sun, °
φ	local latitude, °N/°S
β	PV panel tilting angle, °
γ	PV azimuth angle, °
ψ	sun azimuth angle, °
γ_{rel}	relative temperature coefficient of the maximum power, %/℃
Y_i	dependent variable = $\frac{GHI_{ground}}{GHI_{satellite}}, \frac{DNI_{ground}}{DNI_{satellite}}, \frac{DHI_{ground}}{DHI_{satellite}}$
f	function
X_i	independent variable = time
β_i	unknown parameters
ε_i	error terms

GHI	Global horizontal irradiance
GTI	Global tilted irradiance
DNI	Direct normal irradiance
DHI	Diffuse horizontal irradiance
PV	Photovoltaic
2D	Two dimensional
NREL	National Renewable Energy Laboratory
NASA	National Aeronautics and Space Administration
ASHRAE	American Society of Heating, Refrigerating and AirConditioning Engineer
DL ratio	Pitch-distance-to-PV-length ratio
HDKR	Hay, Davies, Klucher, and Reindl
RESI	Reduced Equivalent Solar Irradiance

LIST OF APPENDICES

CHAPTER 1

INTRODUCTION

1.1 General Introduction

Every hour of sunlight on Earth provides enough energy to meet global energy needs for a year. Unlike fossil fuels, solar energy does not emit harmful gases, making it a sustainable, carbon-free solution crucial for mitigating climate change and minimizing environmental damage. With continual advancements in solar technology, solar power efficiency is expected to rise, making it a lucrative long-term investment.

The renewable energy industry is rapidly growing, as evidenced by data from the International Energy Agency. One driving force behind this growth is the geopolitical shift caused by Russia's invasion of Ukraine, leading European leaders to prioritize renewable energy as a secure alternative to Russian fossil fuels. Political support, increasing energy security concerns, and declining renewable energy costs are opening doors for sustainable development globally. As illustrated in Figure 1.1, solar energy's share of the global energy supply is increasing, accounting for over 50% of the total electricity capacity, signalling a promising trend for solar energy's role in sustainable energy provision. (Levitskiy, 2023)

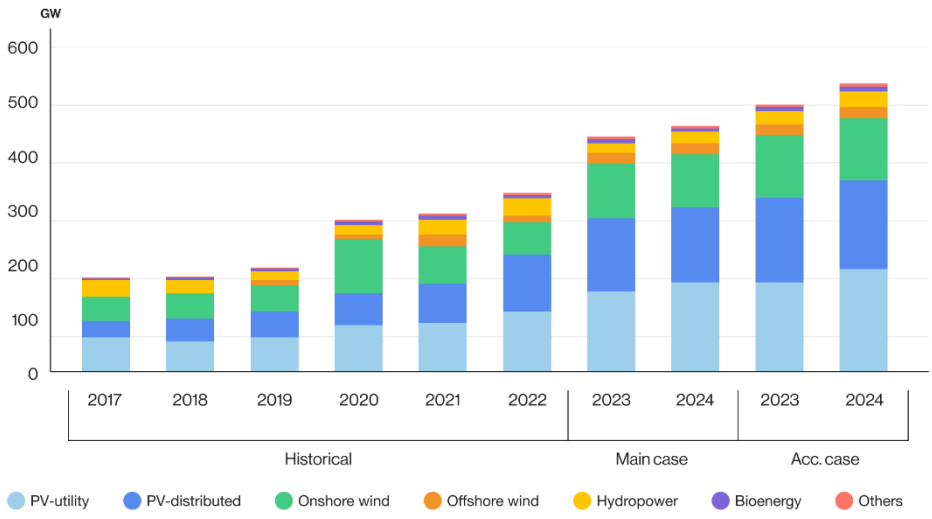

Figure 1.1: Net renewable electricity capacity additions by technology, historical, main, and accelerated cases. (Levitskiy, 2023)

Under such competitive pressure, while solar energy is abundant, maximizing the energy conversion efficiency of PV systems in limited space to produce the most energy output is a primary focus for many PV designers today. Generally, to maximize energy conversion, the most direct approach is to increase the intensity of sunlight. Unfortunately, this isn't something we can control. The sun's position changes constantly due to Earth's rotation, causing variations in sunlight exposure to solar panels throughout the day. Unlike living organisms like sunflowers that track the sun's path, using external motors to drive solar panel tracking would contradict our initial goal as it consumes extra energy. Therefore, finding the optimal yearly angles and orientations for PV systems is crucial.

However, atmospheric particles like weather conditions, air mass, and atmospheric contents continuously affect the distribution of direct and scattered sunlight. For instance, clouds can block direct sunlight, while precipitation like rain, snow, or hail can obstruct sunlight, reducing solar irradiance levels and affecting energy generation. Additionally, atmospheric properties such as aerosols, particulate matter, and gases can attenuate sunlight before it reaches the Earth's surface, significantly impacting solar energy generation.

Moreover, Earth's declination angle leads to seasonal variations in the temperate zones of the northern and southern hemispheres due to the shifting position of the sun's direct rays. This makes finding the optimal angle for solar panels challenging. Furthermore, Earth's elliptical orbit around the sun, combined with obliquity (tilt of the Earth's axis) and precession (wobble of the Earth's axis), affects solar radiation distribution differently at various moments, contributing to long-term climate cycles known as Milankovitch cycles. These cycles influence global climate patterns, including glacial cycles and changes in solar radiation's seasonal distribution.

Additionally, in large-scale solar farms, the arrangement of rows is unavoidable. However, if the tilt angle is too high, it may cast shadows from the front rows of PV arrays onto the ones behind, especially noticeable during early morning and late evening hours. This phenomenon becomes more pronounced in larger PV systems. Therefore, interrow spacing becomes the third variable that needs consideration. This relates to how to find the optimal tilt angle,

placement direction, and interrow spacing distance within limited space. Furthermore, this study also considers the impact of temperature on solar panels, which can reduce overall energy conversion efficiency.

Additionally, the intensity of sunlight received by solar panels is influenced by the latitude of the installation location. Generally, we consider the latitude angle as the optimal tilt angle, with solar panels facing the equator in the northern and southern hemispheres.

1.2 Importance of the Study

This research on the optimal tilt angle and orientation for photovoltaic (PV) systems is crucial for maximizing energy yield, particularly in tropical regions. By optimizing the relevant parameters, solar radiation absorption by PV panels can be significantly increased, leading to higher electricity production.

The significance of this study is reflected in both economic and environmental aspects:

- Maximizes Power Output and Profitability: By optimizing the tilt angle and orientation, PV panels capture the maximum possible sunlight throughout the year, increasing energy output and potentially boosting profitability.
- Reduces Energy Waste: Enhanced energy capture reduces reliance on non-renewable energy sources, contributing to lower carbon emissions and promoting sustainability.
- Tropical Climate Adaptation: This study addresses the specific challenges of tropical climates, where high solar irradiance is counterbalanced by frequent cloud cover and fluctuating seasonal patterns. Optimized PV systems can adapt to these conditions for better performance.
- Minimizes Shading Effects: The research also examines shading, which is particularly critical in large PV installations. By optimizing interrow spacing, shading impacts can be minimized, leading to more efficient land use and higher overall system efficiency.

Additionally, the study employs the Perez model, an advanced sky model that considers factors such as diffuse radiation, cloud cover, and seasonal variations. This model enhances the accuracy of the findings, allowing for precise

determination of the optimal tilt angles and orientations across different locations and timeframes. By addressing these factors, the study aims to improve energy yield, reduce costs, and promote sustainability in PV system installations.

1.3 Problem Statement

Based on the project's continuity from Chong B.Y. (2023), the problem statement can be refined to aim at enhancing the research in the following ways:

- Expanding Location Scope: Chong B.Y. only focused on one specific location, the University of Tunku Abdul Rahman (UTAR), Sg Long Campus in Kajang, Selangor (3.0396 °N, 101.7942 °E). To enhance the validity of the research, the project aims to evaluate optimal parameters across multiple locations.
- Consideration of Orientation Variation: Many researchers in tropical regions have provided varying optimal tilt angles, but they often only consider orientations facing the equator. This project seeks to explore optimal parameters considering a wider range of orientations, acknowledging that optimal orientation may differ based on geographic location and local conditions.
- Advanced Sky Models: Some researchers have utilized simple isotropic models for sky conditions, which may not accurately estimate the diffuse component irradiance absorbed on slanted surfaces. This project aims to incorporate more sophisticated sky models to improve the accuracy of irradiance estimation, leading to more precise optimal parameters determination.
- Comprehensive Regression Relations: While many researchers have established regression relations of optimal tilt angles with other corresponding methods, they often rely on different empirical data and consider few locations. This project aims to develop comprehensive regression relations based on a broader range of empirical data and considering multiple locations to enhance the generalizability of the findings.

1.4 Aim and Objectives

The project aims to correlate latitude with optimal parameters using various types of measured databases. The detailed objectives are listed as follows:

1. To investigate the optimal tilt angle and orientation of photovoltaic modules within tropical regions, using satellite-derived and ground-based measurement solar irradiance databases.
2. To investigate the relationship of solar irradiance at optimal tilting and orientation angles with the design parameters such as interrow spacing, latitude angle, PV panel orientation etc. .

1.5 Scope and Limitation of the Study

In this project, the aim is to correlate the optimal tilt angle and orientation of the PV system with the location's latitude. The Perez sky model is utilized for this purpose. Additionally, interrow spacing is treated as a manipulated variable due to the consideration of a 2D approach for the shadow factor. The project also takes into account the temperature effect. The calculations involved in this study are conducted through simulations contributed by Chong B.Y. (2023). Subsequently, the regression relation can be identified and further developed using a relevant mathematical model.

The limitations of this project are shown as:

1. Geographic Scope: The research is confined to Malaysia and other northern tropical regions, which limits the generalizability of the findings to southern tropical regions where solar irradiance patterns and weather conditions may differ significantly.
2. Reliance on Simulated Data: The study predominantly utilizes simulated data from SolarGIS and PVGIS databases. While these are reputable sources, the reliance on simulations introduces limitations, as they may not fully capture real-world complexities, such as localized shading, micro-climates, and variations in panel performance.
3. The sites selected for this investigation are predominantly located within latitudes 1° to 7°, resulting in an uneven distribution of data points across different latitudes. This uneven distribution introduces a bias toward low-latitude tropical regions, which may affect the accuracy and generalizability of the resultant regression relationship.

4. Simplified Shading Model: The shading model applied in this project assumes the absence of slant shadows on PV arrays. In real-world scenarios, shading conditions are often more complex, particularly in installations with irregular topography or nearby structures, which may affect the accuracy of the derived optimal parameters.
5. Limited Experimental Validation: Although experimental data from Goh's setup in 2024 was used, the validation period only spans from March to September. Extending the experimental validation to a full year would provide a more comprehensive assessment, capturing seasonal variations and improving the robustness of the findings.
6. Fixed Tilt Angle in Experimental Setup: The experimental setup employs a fixed tilt angle of 10°, limiting the investigation to a static configuration. The inclusion of variable tilt angles could allow for a more accurate comparison with simulation results, which account for a range of tilt angles.
7. Limited Economic Considerations: The study primarily focuses on maximizing GTI yield, without integrating economic factors such as installation costs, maintenance, and payback periods. Incorporating a techno-economic analysis would enhance the practical applicability of the findings for real-world PV system deployment.

1.6 Contribution of the Study

The study makes several key contributions to the understanding and optimization of PV systems in tropical regions. It conducts a comprehensive analysis of optimal tilt angle, orientation, and DL ratio, incorporating shading effects, and providing critical insights for PV system design. By comparing SolarGIS and PVGIS simulation data, the research highlights the relative strengths and limitations of these databases, offering valuable guidance for selecting appropriate data sources in different locations. The study also provides practical recommendations for PV system designers, emphasizing latitude, shading, and weather patterns, making the findings actionable for real-world applications. Additionally, the research challenges the general assumption of south-facing orientations for tropical PV systems, advocating for site-specific optimizations based on solar trajectory and local conditions. Overall, the study advances the understanding of tropical PV systems and underscores the

importance of tailored design strategies for improving energy yield in these environments.

1.7 Outline of the Report

In this report, five main chapters present the study on the optimal orientation and tilt angle of photovoltaic (PV) panels, considering factors such as latitude, shading, and different panel configurations.

Chapter 1 introduces the importance of solar energy, particularly in regions with high solar exposure. It explains the need for optimizing the tilt angle and orientation of PV panels to maximize energy output. The chapter outlines the scope of the study and highlights the relevance of finding the best panel configurations for efficient solar energy harvesting.

Chapter 2 provides a literature review, beginning with a discussion of key terminologies related to solar panel performance. It reviews previous research on the optimal tilt angle and orientation of PV panels, as well as methodologies for solar data collection. The chapter also examines models, such as SolarGIS and PVGIS, and the impact of shading and panel configuration on energy efficiency.

Chapter 3 outlines the work plan and methodology used in the study. This includes data collection from SolarGIS and PVGIS databases, processing techniques, and the modeling of the optimal tilt angle based on latitude. The chapter also discusses the methods used to analyze the effect of shading, interrow spacing (DL ratio), and different panel configurations on energy output.

Chapter 4 presents the results and discussion, focusing on the impact of latitude on the optimal tilt angle and orientation of PV panels in tropical regions. It compares simulation results from SolarGIS and PVGIS with experimental data. Additionally, the effects of the DL ratio and different panel configurations (landscape and portrait) on optimal parameters are analyzed.

Chapter 5 concludes the report by summarizing the key findings, including the most effective tilt angles and orientations for PV panels in tropical regions. It also provides recommendations for future research, focusing on improving PV system efficiency.

CHAPTER 2

LITERATURE REVIEW

2.1 Introduction

This project aims to explore satellite and ground-based data differences, understand how solar irradiance impacts PV system performance, and introduce sky models for estimating the diffuse component's distribution. It also references relevant past projects to highlight the topic's importance.

This chapter delves into the distinctions between satellite-derived and ground-based measured databases, discusses various sky models, and provides a comprehensive literature review of related research.

2.2 Literature Review

2.2.1 Solar resource and database

Solar resource data is typically collected and stored in solar databases. These databases compile information about solar radiation levels, including direct and diffuse components, along with meteorological data such as global horizontal irradiation, direct normal irradiation, diffuse horizontal irradiation, sun altitude (elevation) angle, sun azimuth angle, air temperature at a certain height, atmospheric pressure, relative humidity, precipitable water, wind speed, and wind direction at a certain height. The data is often gathered from ground-based measurement stations, satellite observations, and numerical weather prediction models.

2.2.1.1 Satellite-based solar databases

Satellite-based solar databases utilize data collected from satellites equipped with sensors capable of measuring solar radiation levels from space. These satellites continuously monitor the Earth's surface, providing comprehensive coverage of solar irradiance on a global scale.

Normally, satellite-derived data requires the estimation process of solar irradiance typically involves employing empirical, physical, or statistical methods. It can involve historical observational data collected from ground-based stations combined with satellite-derived measurements, detailed

knowledge of atmospheric physics and radiative transfer processes to simulate solar irradiance, and analyzing large datasets of satellite-derived information, such as cloud cover patterns, historical weather patterns, and solar radiation measurements. Then, the statistical techniques are utilized to develop relationships between satellite-derived parameters and observed solar irradiance. By calibrating satellite data against ground measurements, this type of data can minimize the deviation of the measured data to provide accurate estimations of solar irradiance at specific locations. It is presented as a time series to illustrate the variations in solar irradiance under unavoidable changing atmospheric factors, with intervals of every 30 minutes or one hour.

To facilitate historical performance reviews, especially for designers optimizing their PV systems, the Typical Meteorological Year (TMY) method is used to summarize the climate characteristics of a typical year, representing long-term irradiance data. It involves compiling and analysing historical meteorological data, typically spanning multiple years, to create a single dataset that represents the typical weather conditions for a specific location over a typical year. This TMY dataset is valuable in providing a standardized set of weather data that can be used for performance simulations, energy yield assessments, system sizing, and optimization of renewable energy projects.

There are multiple satellite-derived solar resource databases like Meteonorm, SolarGis, PVGIS, SolarAnywhere, NREL / NASA /WhiteBox, and ASHRAE. Each of them has its strengths and weaknesses one their measured method and derived simulation as shown in Table 2.1.

Table 2.1: Satellite-derived solar resource databases.

Database	Spatial resolution	Temporal resolution	Derived model	Remark
Meteonorm	1 km x 1 km	2 min	Hofmann model + Meteotest	Includes weather stations and satellite data
SolarGis	250 m x 250 m	10/15/30 min	Perez's Semi Empirical Satellite Model	Maps and annual solar insolation (including

				TS and TMY data)
PVGIS	1 km x 1 km	1 h	-	Free
SolarAnywhere	3.16 km x 3.16 km	10/15/30 min	Perez model (SUNY)	-
NREL / NASA /WhiteBox, ASHRAE	1 deg. x 1 deg.	1 h	-	-

2.2.1.2 Ground-based solar database

Ground-mounted solar databases rely on ground-based measurements obtained from various monitoring stations, weather stations, and solar radiation sensors installed at specific locations on the Earth's surface. For example, the pyranometer and pyrheliometer are commonly used to measure solar radiation. The pyranometer measures total irradiance, including direct and diffuse sunlight, at the horizontal plane, known as global horizontal irradiance (GHI). In contrast, the pyrheliometer measures the intensity of the direct sunlight component at the normal plane, known as direct normal irradiance (DNI). To obtain the diffuse horizontal irradiance (DHI), the difference between the GHI and DNI is directly calculated. The schematic illustration of a pyranometer and a pyrheliometer are displayed as shown in Figure 2.1.

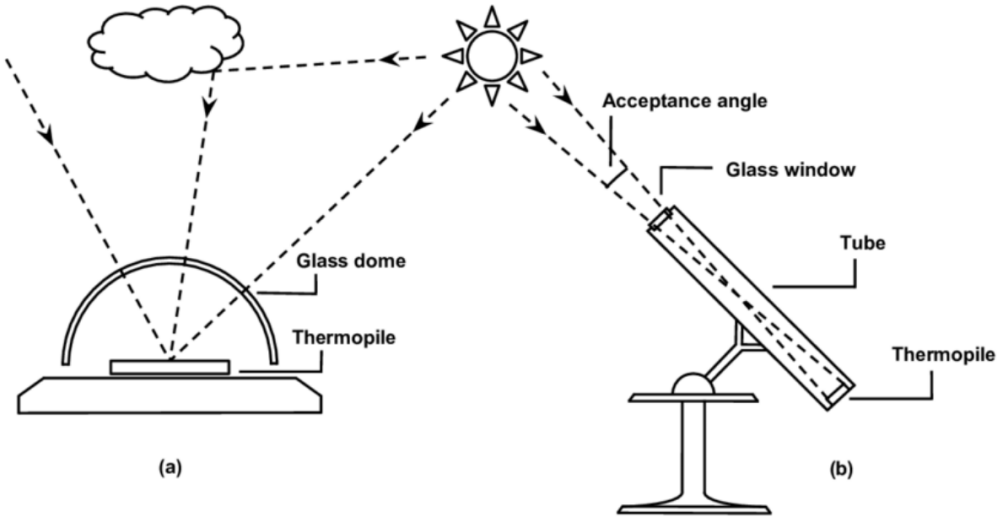

Figure 2.1: A schematic illustration of a pyranometer (a) and a pyrheliometer (b), adapted from Beckman (1997) and Paulescu et al. (2012), respectively.

One of the reasons for the requirement for installing measurement devices together stems from the high likelihood of missing data in ground-measured datasets. This creates a potential trade-off situation. As the daily maintenance is impractical, it is no guarantee of data integrity. Furthermore, errors can occur due to various factors such as the instrument itself, the setup of the entire system, cosine and azimuth effects, temperature response, spectral sensitivity, stability, non-linearity, sun tracking or shade-ring misalignment, instrument leveling, cabling, data logging and transfer issues, environmental factors like dust, snow, water droplets, frost, bird droppings, shading from structures or vegetation, as well as mechanical or electrical field effects, and system shutdowns. Therefore, combining measurements for at least two parameters and conducting internal consistency tests can help reduce database uncertainties (Cebecauer and Šúri, 2016).

One thing to be taken note of is this project considers the shading effect on solar cells. When shaded, solar cells may not receive energy from direct sunlight, but they can still convert energy from the diffuse component into electricity. This highlights the need for different ground-based measurement

devices to be installed for accurate data collection, especially when comparing derived solar irradiance with satellite-based measurements.

As satellite-derived databases rely on empirical data and well-derived statistical algorithms for forecasting, there is still an unavoidable deviation from exact data. Therefore, ground-measured databases play a crucial role in correcting errors by comparing them with actual measured data. This is because ground-mounted measurement devices are installed at specific locations to capture specific climate data. Additionally, these devices offer high memory and real-time recording intervals of 2/5/15/30 minutes, depending on the sensors, providing a high temporal resolution. The comparison between satellite-derived and ground-based databases is presented in a tabular form as shown in Table 2.2.

Table 2.2: The comparison between satellite-derived and ground-based databases.

Aspect	**Satellite-Derived Database**	**Ground-Based Database**
Data Collection Method	Utilizes satellite instruments (radiometers)	Relies on sensors installed on the Earth's surface
Spatial Coverage	Global or large geographic areas	Specific locations where sensors are installed
Temporal Resolution	High temporal resolution (hours to years)	Real-time (minutely), hourly, daily, or monthly data depending on the sensors
Accuracy and Validation	Rigorous calibration and validation processes	Direct measurement for high accuracy, used for validation

Cost and Accessibility	Costly data acquisition, but many databases are free	Initial equipment costs, maintenance, variable data access

2.2.2 Sky model

When solar radiation's direct component traverses the atmosphere, clouds predominantly obstruct it, making the diffuse component more significant, especially in cloudy conditions. Sky models are introduced to mathematically represent the distribution of diffuse component irradiance across various atmospheric conditions. This section details common sky models used in solar system designations, such as the Liu and Jordan model, Klucher model, Hay and Davies model, Reindl model, Muneer model, and Perez models.

2.2.2.1 Liu and Jordan model

Hottel and Woertz (1942) first proposed the isotropic sky model. Following that, Liu and Jordan in 1960 introduced one of the most basic approaches to modeling diffuse radiation. This model simplifies the distribution of diffuse radiation by assuming uniform spread across the entire sky dome and diffuse ground reflection. For surfaces inclined at a tilt angle β from the horizontal plane, the total solar irradiance is expressed as shown in Eqn. (2.1):

$$I_T = DNI \cdot R_b + DHI \cdot \frac{1+cos\beta}{2} + DHI \cdot \rho \cdot \frac{1-cos\beta}{2} \qquad (2.1)$$

where

DNI = direct normal irradiance on a horizontal surface, W/m^2

DHI = diffuse horizontal irradiance, W/m^2

β = tilting angle of the PV system, °

2.2.2.2 Klucher model

In 1979, Klucher observed that when using the isotropic model to calculate the diffuse component irradiance, it tended to underestimate irradiance levels during clear and partly overcast conditions. This phenomenon particularly

occurs when sunlight is at heightened intensity near the horizon and in the circumsolar region of the sky. This implies the neglect of some components of the diffuse sunlight. To address this issue, Klucher developed an alternative model and provided the total irradiance on the tilted surface as shown in Eqn. (2.2).

$$I_T = DNI \times R_b + DHI \times \frac{1+cos\beta}{2}\left[1 + F' \sin^3\left(\frac{\beta}{2}\right)\right] \times [1 + F' \cos^2\theta \sin^3\theta_z] + DHI \times \rho \times \frac{1-cos\beta}{2} \quad (2.2)$$

$$F' = 1 - \left(\frac{DHI}{GHI}\right)^2 \quad (2.3)$$

where

F’ = clearness index in Klucher model

θ_z = solar zenith angle, °

GHI = global horizontal irradiance, W/m^2

The diffuse component of the sky model considers two additional factors. The first factor is the phenomenon of increased diffuse radiation intensity near the horizon, known as the horizontal brightening effect. This phenomenon is particularly prominent under clear or partly cloudy skies. It occurs due to the expansion theory from the principle of diffuse sunlight scattering with air particles in the atmosphere. In the real world, atmospheric scattering can occur in different directions, and the curvature of the Earth can further affect the path length of sunlight through the atmosphere, resulting in different wavelengths. This scattering contributes to the brightness, known as Rayleigh scattering. The intensity of Rayleigh scattering is inversely proportional to the fourth power of the wavelength as shown in Eqn. (2.4). This means that shorter wavelengths (blue and violet) are scattered much more strongly than longer wavelengths (red and orange). (Matan, 2024)

$$I(\theta) = I_0 \left(\frac{R^6}{r^2}\right) (1 + \cos^2\theta) (\lambda^{-4}) \quad (2.4)$$

where

$I(\theta)$ = intensity of scattered light at angle θ, W/m^2

I_0 = intensity of the incident light, W/m^2

R = size of the scattering particles, m

r = distance between the scattering particle and the observer, m

θ = angle between the incident light and the scattered light, °

λ = wavelength of the incident light, nm

Through Eqn. (2.5), the intensity of the scattered light is also inversely proportional to the distance between the scattering particles and the observer. Therefore, near the zenith (directly overhead), the sky appears darkest blue because sunlight has to pass through a relatively small thickness of the atmosphere, resulting in less scattering. However, near the horizon, the path length of sunlight through the atmosphere is much longer. In other words, the curvature of the Earth affects the path length of sunlight as it travels through the atmosphere. Consequently, this increased path length can result in additional scattering and absorption of sunlight, leading to a greater intensity of scattered light (diffuse sunlight) near the horizon.

The second factor is the effect of circumsolar radiation. Generally, when we consider direct component irradiance, the energy absorption area is called the solar disc within a few degrees of the central angle of the sector (in 2D). However, when we consider the particle nature of light, photons have uncertainty in their location. While most of the solar energy received on Earth comes directly from the solar disk, circumsolar radiation includes photons that come from slightly outside the solar disk's edge. This can significantly affect the overall distribution of diffuse radiation in the sky.

In the case of cloudy skies, the clarity index in the Klucher model becomes zero, indicating that the ratio of GHI to DHI is 1. In other words, DNI contributes almost no energy to solar panels. At this point, the model simplifies to an isotropic model. The distribution of diffuse radiation in the sky is assumed to be uniform, consistent with the assumptions of the isotropic model. Both the horizontal brightening effect and circumsolar radiation are related to direct solar radiation, but they have a quantitative impact on diffuse solar radiation.

2.2.2.3 Hay and Davies Sky Model

In the Hay–Davies model, which was introduced by Hay and Davies in 1980, diffuse radiation from the sky is characterized by two main components: the isotropic component and the circumsolar component. Unlike the Klucher model, the Hay–Davies model does not explicitly consider horizon-brightening effects. Instead, it focuses on modeling the distribution of diffuse radiation based on empirical formulations derived from observational data.

Hay–Davies model defined the anisotropy index as A, which plays a crucial role in quantifying the transmittance of beam radiation through the atmosphere as shown in Eqn. (2.5). This index provides insights into the directional distribution of solar radiation, particularly in terms of how it interacts with atmospheric components such as gases, aerosols, and clouds.

$$A = \frac{DNI}{I_{on}} \tag{2.5}$$

where

I_{on} = direct extraterrestrial normal irradiance, W/m^2

The anisotropy index is defined as the ratio of the direct-normal solar irradiance to the direct extraterrestrial normal irradiance. The direct extraterrestrial normal irradiance indicates the solar radiation that would be received on a surface outside the Earth's atmosphere, perpendicular to the sun's rays. Therefore, a higher anisotropy index indicates that a larger proportion of the diffuse radiation is concentrated near the sun, while a lower index suggests a more uniform distribution of diffuse radiation across the sky dome.

The total irradiance is then computed in Eqn. (2.6).

$$I_T = (DNI + DHI \times A)R_b + DHI\left(\frac{1+cos\beta}{2}\right)(1 - A) + DHI\left(\frac{1-cos\beta}{2}\right)\rho \tag{2.6}$$

Indeed, this model integrates spectral analysis techniques to address the wavelength-dependent behavior of solar radiation during its interaction with atmospheric elements. This facilitates a deeper comprehension of how various light wavelengths propagate through the atmosphere, accounting for scattering, absorption, and transmission phenomena. The Hay and Davies method takes

clouds and aerosols, such as dust, pollution, and other particles, into account. This approach is similar to the Liu and Jordan model. Through the parameterization approaches and empirical formulations based on observational data, the model characterizes the interactions between solar radiation components and important atmospheric properties such as aerosol concentration, cloud cover, and optical thickness.

2.2.2.4 Reindl model

The Reindl sky model, developed by Reindl et al., includes components other than isotropic diffuse and circumsolar radiation. Specifically, it considers horizon brightening, as described in their 1990 papers. In addition, the model makes use of the anisotropy index A, which is defined in the same way as the Hay and Davies sky model.

The combination of these components enables the Reindl model to compute total irradiance on a slanted surface as shown in Eqn. (2.7).

$$I_T = (DNI + DHI \times A)R_b + DHI\left(\frac{1+cos\beta}{2}\right)(1-A)\left[1+\sqrt{\frac{DNI}{GHI}}\sin^3\left(\frac{\beta}{2}\right)\right] + DHI\left(\frac{1-cos\beta}{2}\right)\rho \quad (2.7)$$

2.2.2.5 Muneer model

Muneer's model, as summarized by Muneer in 1997, focused on differentiating between shaded and sunlit surfaces under both overcast and non-overcast conditions. This distinction acknowledged that these areas receive varying levels of solar irradiance based on their exposure to direct sunlight.

To quantify the influence of surface tilt on solar irradiance, Muneer's model introduced a tilt factor (T_F), which represented the ratio of the slope background diffuse irradiance to the horizontal diffuse irradiance. This tilt factor is calculated using Eqn. (2.8):

$$T_F = \left(\frac{1+cos\beta}{2}\right) + \frac{2B}{\pi(3+2B)} \times \left[sin\beta - \beta cos\beta - \pi \sin^2\frac{\beta}{2}\right] \quad (2.8)$$

where

B = radiation distribution index

It offers a way to explain the difference between diffuse irradiance on tilted surfaces and horizontal surfaces. The model provides a more precise estimate of the distribution of solar radiation on inclined surfaces by taking into account the slope orientation and its effect on diffuse irradiance.

For surfaces in shade and sunlit surfaces under overcast sky conditions, the total radiation on a tilted plane is:

$$I_T = DNI \times R_b + DHI \times T_F + DHI \left(\frac{1-cos\beta}{2}\right)\rho \qquad (2.9)$$

For surfaces in shade and sunlit surfaces under non-overcast sky conditions, the total radiation on a tilted plane is:

$$I_T = DNI \times R_b + DHI[T_F(1-A) + AR_b] + DHI \left(\frac{1-cos\beta}{2}\right)\rho (2.10)$$

Muneer's model takes into consideration the anisotropy index in non-overcast settings, or situations where direct sunshine is prominent. This index measures the percentage of diffuse radiation that is considered circumsolar, indicating how direct sunlight affects the diffuse radiation pattern as a whole. The anisotropy index is incorporated into the model to account for the differences in diffuse radiation intensity that occur in different regions of the sky dome, especially in areas that are directly affected by the location of the sun.

On the other hand, Muneer's approach makes the formulation simpler when there is cloud cover and direct sunlight is blocked, as it disregards the anisotropy index. This choice is probably motivated by the fact that diffuse radiation takes center stage in cloudy conditions, negating the importance of direct sunshine. In such cases, the distinction between circumsolar and isotropic diffuse radiation may not be as relevant, as the diffuse radiation is more uniformly distributed across the sky dome due to scattering by clouds.

2.2.2.6 Perez model

The Perez sky model, developed by Dr. Richard Perez and his colleagues in 1990, is a widely used solar radiation model that provides a comprehensive framework for estimating solar irradiance under various sky conditions. The

Perez model stands out for its complete approach to simulating solar radiation, particularly its in-depth consideration of various constituents such as isotropic diffuse, circumsolar, and horizon brightening radiation.

The Perez model depends on empirically derived coefficients, which leads to a more accurate depiction of solar irradiance across various sky conditions than some other models that use parameterizations or simplifying assumptions.

In their research, the Perez model provides an intricate dissection of the total irradiance into its parts by examining the distribution of solar radiation over slanted surfaces.

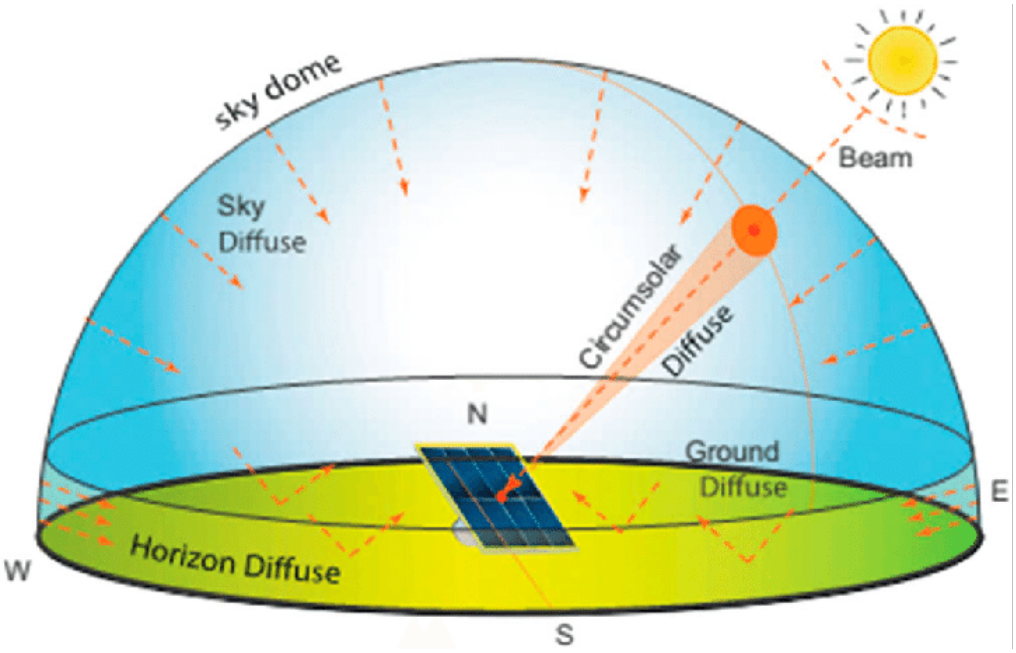

Figure 2.2: Diffuse components of solar radiation in the Perez Model. (Sameti and Jokar, 2016)

Generally, it takes into account two factors: the diffuse component (Figure 2.2), which includes isotropic diffuse radiation, circumsolar radiation, and horizon brightening, and the direct component, which takes into account the angle of incidence of direct sunlight. The reflected portion of the ground-based irradiance is included in the model.

2.2.2.7 Overview of sky models

Comparing these sky models as listed in Table 2.4 supports our decision to apply the Perez model. This model stands out due to its comprehensive consideration of atmospheric conditions, aerosols, and sky conditions, making it highly accurate and suitable for detailed solar energy assessments compared to other models.

Table 2.3: Overview of Solar Radiation Models.

Model	Key Features
Liu and Jordan model	- Based on physical principles - Considers solar position and atmospheric parameters
Klucher model	- Empirical model based on measurements - Considers clearness index and atmospheric conditions
Hay and Davies Sky Model	- Empirical model based on clear sky conditions - Accounts for solar position and aerosol optical depth
Reindl model	- Empirical model based on measurements - Includes diffuse and direct radiation components
Muneer model	- Empirical model with multiple variations - Considers geographical and atmospheric parameters
Perez model	- Statistical model based on measured data - Accounts for sky conditions and aerosol optical depth

2.2.3 Overview of optimum tilt angle determination methods

In the previous section, we know that the tilted angle of the PV panel can vary the effective energy absorption area for the direct component of irradiance. The diffuse component of irradiance is important for contributing energy consistently, especially under overcast conditions. From the derived mathematical model of total tilted irradiance, we realize that the tilted angle and orientation of the PV array are the main manipulated factors in maximizing the energy yield of the PV system. Therefore, many PV designers aim to find the

optimal tilted angle and orientation to maximize the power performance of the PV system.

George and Anto (2012) utilized the Liu and Jordan sky model to estimate the diffused radiation. The location chosen was Kerala, India (9.55°N, 76.81°E). The optimal tilt angle for a PV panel was theoretically estimated for each month using the geographic factor method, clearness index method, and declination angle method.

For the geographic factor method, it can be represented by Eqn. (2.11).

$$R_\beta = \frac{Total\ radiation\ \ on\ the\ tilted\ surface}{Total\ radiation\ \ on\ a\ horizontal\ \ surface} \tag{2.11}$$

where

R_β = geographic factor

Through this method, the tilting angle can be evaluated as the angle that yields the highest value of R_β over the specific period, corresponding to the optimum tilt angle.

Additionally, it introduced the clearness index, K, as the ratio of the Earth's surface global irradiance to the extraterrestrial global irradiance. Then, the following correlation was developed to find the optimal tilting angle as shown in Eqn. (2.12):

$$\beta_{opt} = (6 - 4.8k + 0.86k^{0.27}\varphi + 0.0021\varphi^2) + \left(31k^{0.37} + 0.094k^{0.46} + 0.00634k^{-1.7\phi^2}\right)\cos[\frac{360}{365}(n + 115)] \tag{2.12}$$

where

β_{opt} = optimal tilted angle of the PV system, °

φ = latitude of location, °

K = clearness index

n = n^{th} day of the year

Then, the regression relation between the optimum tilt angle and the declination was listed as Eqn. (2.13), (2.14), (2.15), and (2.16) (Tiris and Tiris, 1998):

$$\beta_{opt} = 33.24 - 1.31(\delta) \quad (2.13)$$

$$\beta_{opt} = 35.15 - 1.37(\delta) - 0.007(\delta^2) \quad (2.14)$$

$$\beta_{opt} = 35.15 - 1.39(\delta) - 0.007(\delta^2) - 4.26 \times 10\text{^}(-5)(\delta^3) \quad (2.15)$$

$$\beta_{opt} = 22.09 + 25.79(K) - 1.49(\delta) \quad (2.16)$$

where

δ = declination angle, °

Eqn. (2.13), (2.14), and (2.15) are the first-order, second-order, and third-order polynomial regression equations respectively. Eqn. (2.16) further correlates the clearness index to the developed function.

As a result, the geographic factor provided the most accurate optimal tilted angle compared to the experimental result. The results imply that the optimum angle varied throughout each month. The highest value of the optimum tilt angle reached 40 degrees, while the lowest optimum tilt angle was 10 degrees. (George and Anto, 2012)

However, this research did not provide the annual optimal tilted angle at that specific location, nor did it consider the orientation of the PV system. Besides that, the sky model considered in this research is an isotropic model, where horizontal brightening and circumsolar radiation are assumed to be zero. This is not precise in practice. Nevertheless, it provides the simplest mathematical model, saving on computation difficulty and time.

Mehleri et al. (2010) used empirical data from the National Technical University of Athens (37°58'N, 23°47'E) to determine the ideal tilting angle and orientation. There were multiple steps in the study. First, data was analyzed to determine the most accurate model, which comprised both isotropic and anisotropic sky models, for estimating solar irradiance on slanted surfaces. Secondly, a database with averages and variations of solar irradiance on tilted surfaces for different times, tilt angles, and orientations was created using the best-selected model and the recorded data. Third, this database was used to

develop metamodels that connected tilt angle and orientation to the variation of the mean global irradiance on tilted surfaces. Finally, using the Neural Network Model (NNM), an optimization problem was created to find the ideal tilt angle and orientation while taking system limitations and constraints into account. However, since the input data was recorded solely from one location, it is important to consider that the findings may have varying impacts when applied to locations at different latitudes.

Asl-Soleimani, Farhangi, and Zabihi (2001) conducted a test to evaluate the actual performance of different types of solar modules at the Department of Electrical and Computer Engineering, University of Tehran, located at latitude 35.7° and longitude 51.4° in Iran. Five sets of solar modules were mounted at tilt angles of 0, 23, 29, 35, and 42°. The results indicated that a tilt angle of around 30° is optimum for grid-connected applications. This finding contradicts the rule of thumb that suggests the optimal tilt angle is equal to the latitude angle. Although Asl-Soleimani, Farhangi, and Zabihi (2001) explored potential factors such as air pollution, further simulations are valuable for verifying the experimental optimal tilt angle conclusively.

Li, Lam, and Chu (2008) experimented at the City University of Hong Kong (latitude = 22.3°N, longitude = 114.2°E). They recorded sky radiance distributions using a sky scanner (EKO MS 300LR) and then utilized the Angstrom-Prescott linear regression equation (Angstrom, 1924; Prescott, 1940) to develop their formulation. The difference between the actual data and the estimated data was below 5.2%. However, it's important to note that the Angstrom-Prescott linear regression equation is based on sunshine hours, limiting its applicability in regions where sunshine hour data are unavailable, especially in remote areas.

Siraki and Pillay (2012) utilized the HDKR anisotropic sky model (Duffie and Beckman, 2006) to estimate irradiation on slanted surfaces at five different latitudes (15 °N, 25 °N, 35 °N, 45 °N, 55 °N). By varying the installation angle, they observed variations in resultant irradiance across months. Additionally, the authors proposed a modified HDKR model to assess how surrounding obstacles affect the optimum tilt angle. The results indicated that for lower latitudes, the optimum angle closely aligned with the location’s latitude, whereas for higher latitudes, the optimum angle was smaller. However,

this observation was valid only for locations with consistent weather conditions and a stable clearness index throughout the year. In reality, locations with highly variable monthly clearness index values may not adhere strictly to this rule. Thus, the authors recommended considering both the location's latitude and the weather conditions during the calculation period when determining the optimum tilt angle.

In Malaysia, Khatib, Mohamed, and Sopian (2012b) utilized the Liu and Jordan model to predict total insolation on tilted surfaces. They conducted their study across five sites in Malaysia: Kuala Lumpur (3.1390°N, 101.6869°E), Johor Bharu (1.4927°N, 103.7414°E), Ipoh (4.5975°N, 101.0901°E), Kuching (1.5495°N, 110.3593°E), and Alor Setar (6.1254°N, 100.3688°E) with the historical data. The research revealed that the optimal tilt angle characteristics for all zones were nearly identical due to Malaysia's seasonal changes. Specifically, the highest optimal tilt angles occurred during the wet season at the beginning and end of the year, while the dry season saw a decrease in optimal tilt angles. The authors provided calculations showing that adjusting the PV module monthly with the corresponding optimal tilt angle resulted in increased yield energy for Kuala Lumpur (5.03%), Johor Bharu (5.02%), Ipoh (5.65%), Kuching (7.96%), and Alor Setar (6.13%). However, the study only considered the PV system's orientations facing south and north, neglecting all-direction changes. Additionally, the use of the simplest isotropic model may have led to significant deviations from actual data due to ideal assumptions. Furthermore, the research did not explore the correlation between latitude and optimal tilt angle.

Ismail et al. (2011) utilized measured data from the Meteorological Station in Chuping Perlis, Perlis (6° 29’ N, 100° 16’ E), to estimate the monthly optimum tilting angle. The research considered the simplest model of diffuse irradiation, assuming that diffuse radiation traveled with equal intensity from all directions under the sky dome. The calculation factored in the beam portion of radiation reaching the Earth's surface (normal to the rays), using the "apparent" extraterrestrial flux and the dimensionless factor known as the optical depth to provide a more accurate value of diffuse horizontal irradiance. In conclusion, the tilt angles of PV modules in Perlis, Northern Malaysia, ranged from −17.16° to 29.74°, where a positive sign indicates south-facing orientation, zero

indicates horizontal placement and a negative sign indicates north-facing orientation of the PV module. However, the study did not consider changes in the PV module's orientation across 360°. The sky model used was not advanced enough to estimate the exact value of diffuse insolation. It only provided the monthly optimum tilted angle, whereas, in certain circumstances, the yearly optimum tilted angle could be more useful.

Tiris and Tiris (1998b) utilized the Liu and Jordan model to formulate a mathematical model for the optimal tilted angle at Gebze (40°47'N, 29°28'E), situated at an altitude of 182 meters above sea level. The model incorporated possible correlations between the optimal tilted angle and factors such as the diffuse-to-total radiation ratio, cloudiness factor, and declination angle. These correlations were evaluated using root-mean-square error (RMSE) and mean-bias error (MBE). Eqn. (2.13), (2.14, (2.15), and (2.16) obtained the minimum errors compared to other models. By substituting the correlated variables with the coefficients, the estimated results indicated that the optimal tilt should be 21.3° in spring, 6.3° in summer, 47.4° in autumn, and 58° in winter. The yearly average tilt was estimated to be 33°. However, this model was developed based on data from a single location. Different latitudes and geographic terrains may lead to different regression relations and resultant coefficients. Additionally, using the Liu and Jordan model and neglecting the effect of the change in orientation of the PV system could result in significant deviations from real-world scenarios.

Skeiker (2009) devised an analytical method to derive a formula with minimal parameters necessary for calculating optimal tilt angle$_t$ on any selected day and latitude, regardless of the hemisphere, and for any given value of γ.

The first step of the derivation was considered the total extraterrestrial radiation received daily by a south-facing surface, tilted at an angle β to the horizon, which can be mathematically expressed as Eqn. (2.17) (El-Kassaby, 1988):

$$I_d = \frac{24}{\pi} I_0 \left[1 + 0.034 \cos\left(\frac{2\pi n}{365}\right)\right] \times \cos(\varphi - \beta)\, cos\delta \sin h_{ss} + h_{ss} \sin(\cos(\varphi - \beta)\, sin\delta \quad (2.17)$$

$$\delta = -23.45 \cos\left[\frac{(n+10.5)360}{365}\right] \quad (2.18)$$

$$h_{ss} = \cos^{-1}[-\tan\varphi \tan\delta] \quad (2.19)$$

where

ϕ = latitude of the location, °N/°S

β = tilt angle of the PV system, °

δ = declination angle, °

h_{ss} = sunset hour angle, °

Then, differentiating the I_d with respect to β at that particular day, which can be expressed in Eqn. (2.20).

$$\frac{dI_0}{d\beta} = 0 \quad (2.20)$$

$$\beta_{opt} = \varphi - \tan^{-1}\left[\frac{h_{ss}}{\sin h_{ss}}\tan\delta\right] \quad (2.21)$$

Considering the one-time change every month, the total irradiance become:

$$I_m = \sum_{n=n_1}^{n=n_2} I_d \quad (2.22)$$

where

m = month number

n_1 = first day of the m^{th} month as counted from January

n_2 = last day of the m^{th} month as counted from January

Therefore, the monthly optimal tilt angle, $\beta_{opt,m}$ and the monthly averaged daily mean sunset hour angle for the tilted surface can be represented as:

$$\beta_{opt,m} = \varphi - \tan^{-1}\left\{\frac{\sum_{n=n_1}^{n=n_2}\frac{24}{\pi}I_0\left[1+0.034\cos\left(\frac{2\pi n}{365}\right)\right]\sin(\delta)h_{ss}}{\sum_{n=n_1}^{n=n_2}\frac{24}{\pi}I_0\left[1+0.034\cos\left(\frac{2\pi n}{365}\right)\right]\cos(\delta)\sin(h_{ss})}\right\} \quad (2.23)$$

$$h_{ss,m} = \min[\cos^{-1}(-\tan\varphi\tan\delta), \cos^{-1}(-\tan(\varphi-\beta)\tan\delta)] \quad (2.24)$$

These equations are designed to determine the optimal tilt angle for a month and calculate the total extraterrestrial insolation. To validate the accuracy of this derived model, the author conducted a comparison with Nijegorodor et al.'s model. Nijegorodor et al. utilized the Hay and Davies model to describe the diffuse irradiance distribution and developed a set of 12 equations for each month individually. Their method estimated the monthly-averaged optimal tilt angle for locations between latitudes of 60° south to 60° north. The comparison revealed a slight difference of up to +/- 5 % between the two methods. This variance can be attributed to the optimization of these equations using mathematical techniques, without considering the localized solar radiation patterns specific to each location.

In 2024, Goh also investigated the optimal orientation of fixed photovoltaic modules on the rooftop of Universiti Tunku Abdul Rahman, Bandar Sungai Long, Kajang, Selangor, Malaysia to maximize electricity generation. The study focuses on optimizing the azimuth angle with a fixed tilt of 10 degrees. Eight PV modules were arranged in an orthogonal configuration (North, North-East, East, South-East, South, South-West, West, and North-West), and data on power output, temperature, and solar irradiance were collected using APSystems Energy Monitoring and Analysis (EMA) software and a custom-built data logging system. The outputs were normalized using the North-East panel as a reference to ensure consistency in performance comparison.

Data analysis revealed that the east-oriented panel consistently achieved the highest electricity generation, followed by the north-east and south-east orientations, while the west-facing panel produced the least. Temperature effects caused an energy loss of approximately 8.6% to 8.9% across all orientations. The findings indicate that the east orientation is optimal for fixed PV panels in Malaysia's tropical climate, emphasizing the importance of accounting for environmental factors such as temperature when designing PV systems. The study did not explore seasonal variations in tilt angle, as a fixed

10-degree tilt was used based on industry practices for dust mitigation, and the data collection spanned only one month (March-April).

2.3 Summary

The literature review indicates a wide range of recommended optimal tilt angles by different authors. Upon detailed analysis of the approaches mentioned above, several observations emerge:

- Some approaches are overly simplified and tailored to specific locations.
- Various atmospheric transmittance models are not accounted for.
- Certain studies overlook the impact of changing the orientation of the PV system in all directions.
- Some approaches only focus on monthly optimal parameters without considering average yearly optimal parameters.
- Skeiker (2009b) derived an analytical model but still exhibited deviations compared to the empirical model established by Nijegorodov et al. (1994).

As a result, this study aims to develop a systematic formula using computational techniques. It will incorporate the Perez sky model, known for providing the most accurate distribution of the diffuse component insolation compared to other sky models. This formula will determine the optimal tilt angle, orientation, and row spacing distance for different latitudes within the tropical region. To further expand this project, the temperature effect and the shading mismatching effect on the PV system are taken into consideration as the maternal project from Chong B.Y. (2023). Then, the experimental orthogonal PV system is measured to prove the simulated result.

Here's a table summarizing the cited authors, research locations, the sky model used (if any), the methods employed, and most importantly, the correlation or resultant optimal tilt angle/orientation based on their findings:

Table 2.4: Summary of the literature review.

Cited Author(s)	**Location**	**Sky Model Used**	**Methods Employed**	**Correlation/Resultant Optimal Tilt/Orientation**
George and Anto (2012)	Kerala, India	Liu and Jordan	Geographic factor method, clearness index method, and declination angle method.	The optimal tilt angle varied monthly, with a maximum of 40° and a minimum of 10°. The study didn't provide an annual optimal tilt or consider orientation.
Mehleri et al. (2010)	Athens, Greece	Isotropic and Anisotropic	Comparison of sky models, database development, metamodel creation, and optimization using a Neural Network Model (NNM).	The study doesn't explicitly state a correlation or specific optimal values. It suggests using their NNM approach for location-specific optimization considering various factors.
Asl-Soleimani et al. (2001)	Tehran, Iran	Not specified	Experimental study analyzing actual performance of solar modules at various tilt angles.	They found an optimal tilt angle of around 30°, suggesting that the optimal tilt might not always equal the latitude.

Li et al. (2008)	Hong Kong	Not specified	Sky radiance distribution recording and application of the Angstrom-Prescott linear regression equation.	The research doesn't provide a specific optimal tilt or orientation, but it emphasizes the correlation between total solar radiation on tilted surfaces and sunshine hours.
Siraki and Pillay (2012)	Five different latitudes	HDKR	Irradiation estimation on slanted surfaces, analysis of tilt angle impact on irradiance, and proposal of a modified HDKR model.	For lower latitudes, the optimal tilt angle aligned closely with latitude; for higher latitudes, the optimal angle was smaller. They recommend considering both latitude and weather conditions.
Khatib et al. (2012b)	Five sites in Malaysia	Liu and Jordan	Total insolation prediction, analysis of monthly optimal tilt angles, and assessment of energy yield improvements with tilt angle adjustments.	Highest optimal tilt angles occurred during the wet season, and adjusting the tilt monthly resulted in energy yield increases ranging from 5.02% to 7.96% depending on the location.
Ismail et al. (2011)	Perlis, Malaysia	Simplified Diffuse Irradiation Model	Calculation of beam radiation and utilization of the optical depth factor for diffuse horizontal irradiance estimation.	The study found monthly optimal tilt angles for PV modules in Perlis, Malaysia, ranging from -17.16° to 29.74° (positive indicates south-facing).

Tiris and Tiris (1998b)	Gebze, Turkey	Liu and Jordan	Mathematical model development considering correlations between optimal angle and radiation ratios, cloudiness, and declination angle.	Developed regression equations relating optimal tilt angle to declination angle and clearness index. The study estimated optimal tilt angles for different seasons, with a yearly average of 33°.
Skeiker (2009)	Various latitudes (global)	Not specified	Analytical method for calculating optimal tilt angle based on latitude, declination angle, and sunset hour angle.	Derived a formula for calculating the optimal tilt angle for any day and latitude, showing a slight difference (up to +/- 5%) compared to the empirical model by Nijegorodov et al. (1994).

CHAPTER 3

METHODOLOGY AND WORK PLAN

3.1 Introduction

This chapter implies the detailed procedures for evaluating the optimal tilting angle and orientation of the photovoltaic (PV) system at different locations with different row spacing distances. All investigated locations are within the tropical region with the typical tropical weather. The Perez sky model is implemented to determine the global tiled irradiance, which contributes to three components direct sunlight, diffuse sunlight, and the sunlight reflected by the ground. The designed PV system is implemented with two rows of the PV arrays in the system and the row spacing distance is further probed with the consideration of the shading effect on the solar module. Besides that, a simple Ross coefficient model is utilized to analyze the module operating temperature, leading to the temperature effect on the solar cell, resulting in the impact on the performance of the PV system.

Moreover, the configurations of the models under study are derived from those established by Chong B. Y. in 2023 through simulation coding. These selected configurations have been meticulously crafted to align with the current design standards for large-scale solar farms (LSS), ensuring that the simulations yield practical and applicable results for real-world implementation.

By comparing the power performance of these configurations in previous projects, it was observed that landscape arrangements involving two or three stacked solar panels were not chosen due to their intermediate values of normalized shading loss under partial shading conditions, as depicted in Figure 3.1. Essentially, the greater the number of stacked solar panels, the more evenly distributed the variations in shading loss become. The same principle applies to portrait arrangements with multiple stacked solar panels.

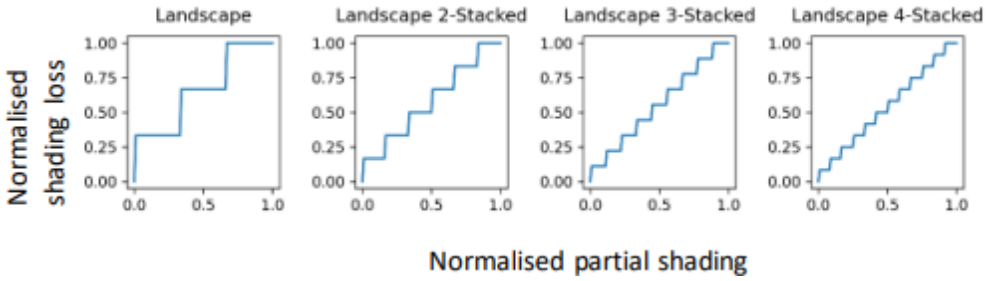

Figure 3.1: Graphs of Shading Loss against Partial Shading for Landscape-oriented PV. (Chong, 2023)

However, the landscape arrangement involving four stacked solar panels remains to be simulated to validate this relationship in the context of this project.

This project requires a lot of simulations to assist in processing the input data and computing the key parameters based on the mathematical model. The used simulation in this project is contributed by Choong B. Y. (2023). Most of the computation tools depend on the built-in functions in the pvlib python library established by F. Holmgren et al. (2018).

3.2 Chosen location

For the chosen locations, they fall within the tropical region between the latitudes of 30 °N and 30 °S, with a specific focus on Malaysia. These locations experience the characteristic tropical climate, which is characterized by consistently warm temperatures throughout the year, minimal seasonal temperature variations, and distinct wet and dry seasons. The tropical climate in these regions is further defined by high humidity levels, intense sunlight, and occasional heavy rainfall. This characteristic can significantly influence the method deviation of summarized Typical Meteorological Year (TMY) irradiance data, particularly in determining the weight factor distribution for solar irradiance, temperature, humidity, wind speed, cloud cover, and atmospheric stability.

Appendix A lists the chosen location for this project.

3.3 Data preprocessing

Due to the uncertainty caused by missing data in ground-based devices, conducting quality assessment tests is crucial. Initially, automatic tests are run to detect obvious issues based on numerical criteria. Subsequently, visual inspection is employed to identify more complex issues that are challenging to describe generically and require significant professional knowledge and expertise from experienced operators.

The automatic quality assessment tests involve identifying missing values and time shifts in the measured data. Additionally, assessing measurements against the sun's position is essential, distinguishing between irradiance contributions mainly from the Moon and other stars after sunset, which can be disregarded. Furthermore, the data is compared with possible minimum and maximum irradiance limits, and the consistency of Global Horizontal Irradiance (GHI), Diffuse Horizontal Irradiance (DIF), and Direct Normal Irradiance (DNI) is evaluated by comparing redundant measurements. (NREL, 1993)

In the visual quality control step, the goal is to identify and flag various erroneous patterns. For instance, shading from nearby objects (near shading) or mountains (far shading) at the measured location can impact the dataset's pattern and needs comparison with regular data error patterns. Moreover, sensor calibration issues may lead to irregular anomalies that require experienced operators to identify. (Younes, Claywell and Muneer, 2005)

Data readings that do not pass the quality assessment tests are flagged and excluded from further analysis, with the remaining data aggregated into hourly time steps.

For the satellite-derived databases, Solargis is mainly selected as the empirical data for computation due to its relatively high spatial and temporal resolution, however, other types of data are randomly chosen for the accuracy comparison purposes.

3.4 Modelling of solar radiation on the tilted surface

The component of incident global solar radiation on a tilted surface (GTI) can be expressed by,

$$I_T = I_B + I_D + I_R \quad (3.1)$$

where

I_T = total incident solar radiation, W/m^2

I_B = direct component of the solar radiation, W/m^2

I_D = diffuse component of the solar radiation, W/m^2

I_R = reflected component of the solar radiation, W/m^2

According to the Perez All-Weather Sky Model (Perez et al., 1987), which is a mathematical model used to describe the relative luminance distribution of the sky dome, the components of sunlight can correlate to their corresponding horizontal irradiance, as shown below:

$$I_T = DNI \cdot R_b + DHI \cdot R_d + DHI \cdot \rho \cdot R_r \quad (3.2)$$

where

R_b = coefficient of the direct component of the solar radiation

R_d = coefficient of the diffuse component of the solar radiation

R_r = coefficient of the reflected component of the solar radiation

ρ = ground Aledo, the reflectance of the ground

3.4.1 Beam component on the tilted surface

The beam component of sunlight, also known as the direct component, is affected by the cosine effect due to the tilt of the solar panel (Figure 3.2). When the sunlight strikes the surface of the solar panel at a certain angle, which is a so-called incident of angle (AOI), the effective area of the solar panel that receives the sunlight decreases due to the oblique angle of the incident sunlight. As a result, the amount of the absorbed energy is reduced. Therefore, the cosine efficiency indicates the coefficient of the direct component of solar radiation.

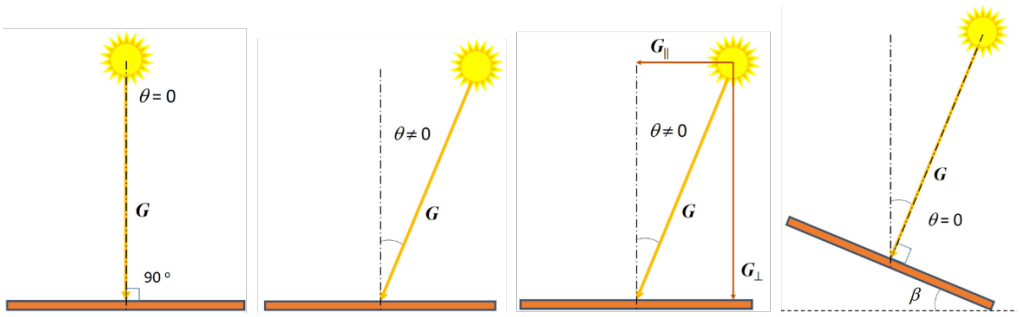

Figure 3.2: Impact of orientation and tilt panel surface on solar energy capture. (Fedkin et al., 2024)

In three-dimensional space, the incident beam of sunlight and the normal incident plane of the solar panel can be represented in vector form. As a thumb of rule, the dot product of two vectors is equal to the product of the magnitude of the two vectors and the cosine of the angle between the two vectors. Mathematically, the cosine effect can be simply represented as:

$$R_b = \cos\theta = \frac{\vec{I}\cdot\vec{N}}{|\vec{I}|\cdot|\vec{N}|} \tag{3.3}$$

where

$\cos\theta$ = cosine efficiency
$\vec{I}$ = solar radiation vector
$\vec{N}$ = normal vector of the PV module surface

To represent them in 3D vector form (Figure 3.3), the sun azimuth angle and altitude angle are introduced. The former is the clockwise angle from true north to the projected sun's position on the horizontal plane on the earth's surface, while the latter is the angle between the direction of the Sun and the horizontal plane. Then, the corresponding zenith angle of the incident, which is the angle between the normal to the horizontal plane at a given location and the incident beam radiation, is derived by Iqbal in 1983 as:

$$\cos\theta_z = \cos\varphi\cos\delta\cos\omega + \sin\varphi\sin\delta \tag{3.4}$$

where

θ_z is the solar zenith angle, °

α is the solar altitude angle, $\alpha = 90° - \theta_z$, °

ω is the hour angle, in the local solar time, °

δ is the current declination of the Sun, °

φ is the local latitude, °N/°S

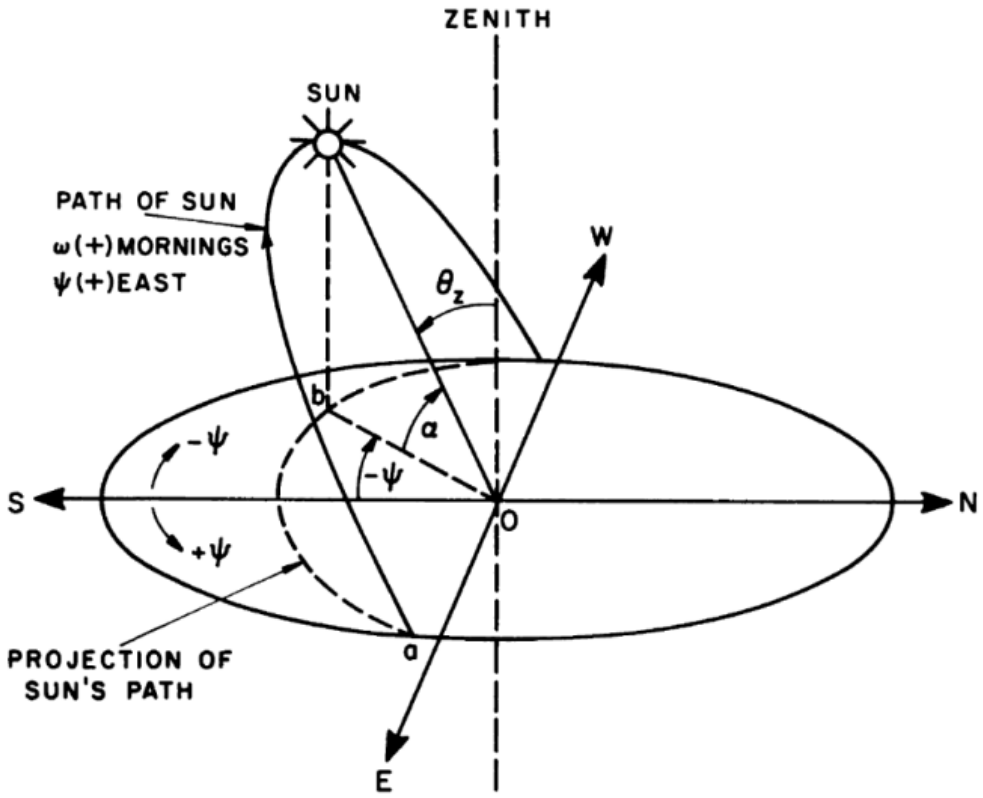

Figure 3.3: Definition of the sun's zenith (θ_z), azimuth (ψ), and altitude (α) angles. (Iqbal, 1983)

Therefore, for a surface oriented in any direction to the local meridian, the trigonometric relation in Eqn. (3.5) or the simplified form in Eqn. (3.6) is solved by Widén and Munkhammar in 2019 as follows:

$$cos\ \theta\ =\ sin\ \delta sin\ \varphi cos\ \beta\ +\ cos\ \delta cos\ \varphi cos\ \beta cos\ \omega + cos\ \delta sin\ \varphi sin\ \beta cos\ \gamma cos\ \omega + cos\ \delta sin\ \beta sin\ \gamma sin\ \omega \quad (3.5)$$

or

$$cos\ \theta\ = cos\beta cos\theta_z + sin\beta sin\theta_z cos(\psi - \gamma) \quad (3.6)$$

where

β = PV panel tilting angle, °

γ = PV azimuth angle, °

3.4.2 Diffuse component on the tilted surface

In Perez's diffuse sky model, it has considered a few factors that contribute to the diffuse sunlight received by the solar module, such as isotropic diffuse, circumsolar, and horizon-brightening radiation. The resultant expression of the diffuse component of the solar irradiance in the Perez model can be denoted as:

$$R_d = (1 - F_1)\left(\frac{1+\cos\beta}{2}\right) + F_1\frac{a}{b} + F_2\sin\beta \tag{3.7}$$

where

F_1 = circumsolar coefficients

F_2 = horizon brightness coefficients

The circumsolar and horizon brightness coefficients are important to capture the additional radiation near the sun's position and the brightness near the horizon, modeling the solar radiation distribution.

The terms "a" and "b" in the model are parameters that account for the incidence angle of the sun on the slope under consideration of circumsolar and horizon-brightening radiation. They help adjust the model predictions based on the orientation and tilt of the surface relative to the position of the sun. The terms a and b are computed using:

$$a = \max(0°, \cos AOI) \tag{3.8}$$

$$b = \max(\cos 85°, \cos\theta_z) \tag{3.9}$$

Besides that, the brightness coefficients F_1 and F_2 depend on the sky condition parameters clearness ε and brightness Δ. These factors are defined as:

$$\varepsilon = \frac{\frac{DNI+DHI}{DHI}+5.535\times10^{-6}\theta_z^3}{1+5.535\times10^{-6}\theta_z^3} \tag{3.10}$$

$$\Delta = m\frac{DNI}{I_0} \tag{3.11}$$

where

m = air mass

I_0 = extraterrestrial radiation, the solar radiation that reaches the Earth's atmosphere from the Sun, W/m^2

The complex equations for clearness ε and brightness Δ coefficients are derived empirically through the regression analysis with the pre-processed collected data under various sky conditions.

The clearness coefficient ε is designed to quantify the atmospheric clarity or transparency, considering both direct and diffuse solar radiation components. Similarly, the brightness coefficient Δ is to characterize the sky's overall brightness, in the sector of the intensity of circumsolar and diffuse radiation components relative to the DNI under the consideration of the effects of atmospheric scattering, aerosols, and other factors influencing the distribution of solar radiation.

F_1 and F_2 are then computed with:

$$F_1 = \max\left[0, \left(f_{11} + f_{12}\Delta + \frac{\pi\theta_z}{180}f_{13}\right)\right] \tag{3.12}$$

$$F_2 = f_{21} + f_{22}\Delta + \frac{\pi\theta_z}{180}f_{23} \tag{3.13}$$

where

f_{ij} = coefficients of the Perez model

The coefficients f_{ij} were obtained through statistical analysis of empirical data collected from specific locations. This analysis involved deriving two distinct sets of coefficients, which are the irradiance coefficient and illuminance coefficient to represent the variability in sky conditions observed across different locations. Table 3.2 shows the coefficients of Perez model for irradiance and illuminance. (Perez et al., 1990)

Table 3.1: Perez model coefficients for irradiance and illuminance. (Perez et al., 1990)

εBin	F_{11}	F_{12}	F_{13}	F_{21}	F_{22}	F_{23}
	IRRADIANCE COEFFICIENTS					
1	-0.008	0.588	-0.062	-0.060	0.072	-0.022
2	0.130	0.683	-0.151	-0.019	0.066	-0.029
3	0.330	0.487	-0.221	0.055	-0.064	-0.026
4	0.568	0.187	-0.295	0.109	-0.152	-0.014
5	0.873	-0.392	-0.362	0.226	-0.462	0.001
6	1.132	-1.237	-0.412	0.288	-0.823	0.056
7	1.060	-1.600	-0.359	0.264	-1.127	0.131
8	0.678	-0.327	-0.250	0.156	-1.377	0.251
	ILLUMINANCE COEFFICIENTS					
1	0.011	0.570	-0.081	-0.095	0.158	-0.018
2	0.429	0.363	-0.307	0.050	0.008	-0.065
3	0.809	-0.054	-0.442	0.181	-0.169	-0.092
4	1.014	-0.252	-0.531	0.275	-0.350	-0.096
5	1.282	-0.420	-0.689	0.380	-0.559	-0.114
6	1.426	-0.653	-0.779	0.425	-0.785	-0.097
7	1.485	-1.214	-0.784	0.411	-0.629	-0.082
8	1.170	-0.300	-0.615	0.518	-1.892	-0.055
Circumsolar Brightening Coefficient				$F_1 = F_{11} + F_{12}*\Delta + F_{13}*Z$		
Horizon Brightening Coefficient				$F_2 = F_{21} + F_{22}*\Delta + F_{23}*Z$		

3.4.3 Reflected component on the tilted surface

The reflected component of solar radiation from the ground depends on the Albedo number, which is the reflectance of the ground based on its material. The relevant coefficient considers the isotropic model, assuming negligible contributions from circumsolar and horizon brightening components. This validity holds for the reflected component due to its high dependency on ground Albedo. Therefore, it can be expressed as follows:

$$R_r = \frac{1-\cos\beta}{2} \tag{3.14}$$

The negative sign in the cosine term is notably taken because this component contributes from the downward direction compared to the diffuse component in the isotropic model.

Regardless of the ground material in different locations, even within specific areas, the ground Albedo can vary throughout the year. This variation is due to seasonal regions experiencing snowy weather, effectively adding an extra reflective surface layer. Consequently, the resulting reflected component fluctuates. However, this project focuses solely on tropical regions, minimizing

the impact of this natural phenomenon. In addition, this project aims to provide industry guidance on implementing PV systems, so the optimal orientation should not include controllable ground surface types, which give different results at different sites. Therefore, ground reflectance is not considered.

3.4.4 Shading effect on beam component of the solar irradiance

In this project, the PV system is designed with two rows of PV arrays. Consequently, there is potential for shading from the front row of arrays on the row behind, especially noticeable during sunrise and sunset. To account for this, a shading factor is introduced to scale down the contribution of the beam component of solar radiation, leading to an overall performance drop due to shading loss. It's important to note that the diffuse and reflected components are not significantly affected by shading due to their basic assembly.

Thereby, the improved beam component of solar radiation can be expressed as follows:

$$I_b = DNI \times R_b \times (1 - f_s) \tag{3.15}$$

where

f_s = shade factor

According to Saint-Drenan and Barbier's derivation in 2019, firstly, we consider the shading area proportional to the shade factor, f_s as defined in Eqn. (3.16), which is also the ratio of the shading length to the whole solar panel length in a 2D simplified model of the PV system with the assumption of the infinite length of each row of solar panels as shown in Figure 3.4. This assumption is to minimize the effect of the small solar incidence angle at sunrise and sunset, leading to the high oblique shade of the shadow blocking the corresponding solar panel and hence one of the terminals (east or west) will be unshaded to contribute to the small electrical generation as usual with the beam sunlight component.

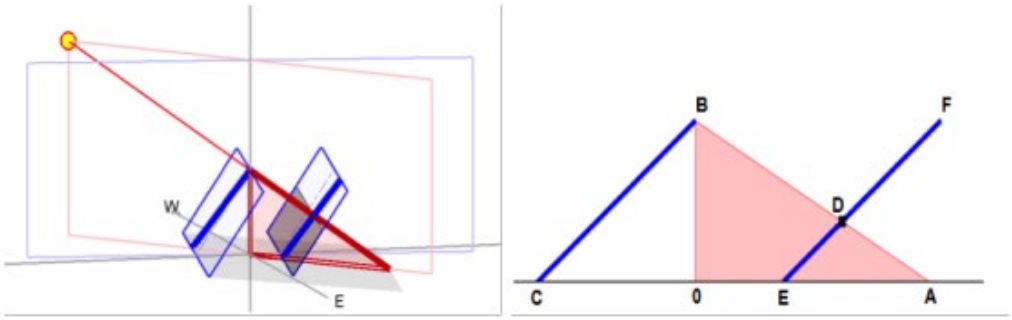

Figure 3.4: Illustration of the lengths used for the calculation of the shaded fraction in the space (left) and in the plane including the sun and the origin (right). (Saint-Drenan and Barbier, 2019)

$$Shading\ factor, f_s = \frac{DF}{DG} \tag{3.16}$$

$$\because AB = DG\ (assumming\ each\ solar\ panel\ have\ the\ same\ length)$$

$$\therefore f_s = \frac{DF}{AB} \tag{3.17}$$

$$\because similar\ triangles, pairs\ of\ corresponding\ sides\ are\ proportional$$

$$\therefore f_s = \frac{DE}{BE} \tag{3.18}$$

Since the PV azimuth angle, γ (the orientation of the PV system) and the solar azimuth angle, ψ can be obtained from the setting value and the measured data, they can be the important variable to assist in the analysis of the impact of the shading effect. In other words, the relation of the shading factor is intended to be represented with the PV azimuth angle, γ and the solar azimuth angle, ψ. Therefore, the shade factor is further converted to the following form:

$$f_s = \frac{CE-CD}{BC+CE} \tag{3.19}$$

Referring to Saint-Drenan and Barbir in 2019, the effective lengths CE, CD, BC, and the resultant f_s can be derived using simple trigonometric theory within the geometry case illustrated below:

$$CD = \frac{d}{\cos(\psi-\gamma)} \tag{3.20}$$

$$CE = \frac{l\sin\beta}{\tan\alpha} \tag{3.21}$$

$$BC = \frac{l\cos\beta}{\cos(\psi-\gamma)} \tag{3.22}$$

$$\therefore f_s = \frac{CE-CD}{BC+CE} = \frac{\frac{l\sin\beta}{\tan\alpha_s}-\frac{d}{\cos(\psi-\gamma)}}{\frac{l\cos\beta}{\cos(\psi-\gamma)}+\frac{l\sin\beta}{\tan\alpha}} \tag{3.23}$$

where

d = the interrow spacing distance between the PV arrays

l = the length of the solar panel

Note that the shading factor will only be valid when $-\frac{\pi}{2} < (\psi-\gamma) < \frac{\pi}{2}$, and it is symmetrical from 0 to $\frac{\pi}{2}$ and $-\frac{\pi}{2}$ to 0. Besides that, from Figure 7.1, we can find out that the shading effect only occurs when the angle ∠BAE is larger than $\frac{\pi}{2}$. In other words, when the $|\alpha-\beta| < \frac{\pi}{2}$, the shading factor should be zero to represent the non-shaded. Therefore, it can be expressed as:

$$f_s = \begin{cases} \frac{\left|\frac{l\sin\beta}{\tan\alpha_s}\right|-\left|\frac{d}{\cos(\psi-\gamma)}\right|}{\left|\frac{l\cos\beta}{\cos(\psi-\gamma)}\right|+\left|\frac{l\sin\beta}{\tan\alpha}\right|}, & if\ |\alpha-\beta| < \frac{\pi}{2} \\ 0, & if\ |\alpha-\beta| < \frac{\pi}{2} \end{cases} \tag{3.24}$$

3.4.5 Reduced Equivalent Solar Irradiance (RESI)

In the previous section, we discussed how the shading factor can reduce the effective absorbing area of a solar panel, thereby lowering the overall performance of the PV system. However, shading losses in solar panels are non-proportional, meaning even a small shading percentage can significantly impact the panel's power output. This is because solar cells within a panel are interconnected (in series), and a shaded cell can limit the maximum current the entire module can achieve, acting as the weakest link.

While bypass diodes can mitigate this effect, they also occupy space and add to costs, posing investment risks. Considering the long-term perspective of this project, with high temporal resolution tracking the sun's trajectory and the gradual changes in shade length, addressing shading issues and the resulting mismatch problem in solar panels becomes crucial for optimizing system performance.

In this project, the simulation is modeled with a simple shading case, assuming no slant shadows on the rows of PV arrays. This simplification is important for simulation ease, considering the reduced equivalent solar irradiance.

Additionally, the project includes three case studies involving different PV module arrangements: a landscape arrangement with four stacked solar panels, a linear landscape arrangement with a single solar panel, and a portrait arrangement with a single panel. The landscape and portrait arrangements can experience significant impacts due to the same shade length. The figure below illustrates the substantial impact of shading on both landscape and portrait arrangements.

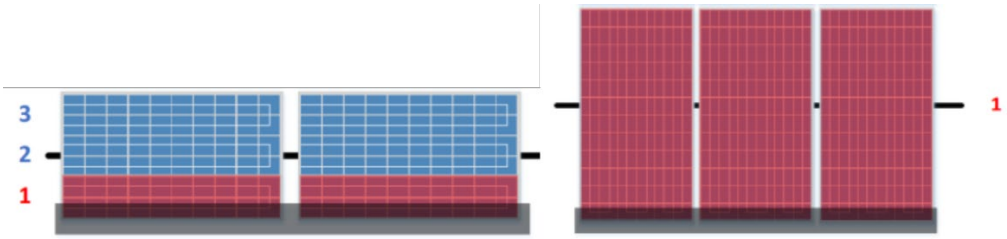

Figure 3.5: Effect of Partial Shading for Different Panel Configurations (Chong and Universiti Tunku Abdul Rahman, 2023)

In Figure 3.5, each solar panel consists of three rows of internally connected solar cells in series and parallel to each other. Each row of solar cells is also connected to a bypass diode. As the shadow length gradually increases from the bottom, the landscape arrangement PV array may have one row of solar cells bypassed by the diode due to low current generation and resulting high resistance. However, the portrait arrangement PV array experiences all rows of solar cells being bypassed, resulting in no electricity generation. This

phenomenon is of interest to PV designers and installers when implementing large-scale solar farms.

3.4.6 Modeling the simulation

In this project, several parameters are studied to understand their relationships: the latitude angle, tilted angle, orientation, and interrow spacing of the PV array. A simulation tool is used to handle the numerous calculations involved. Initially, key input parameters such as Direct Normal Irradiance (DNI), Diffuse Horizontal Irradiance (DHI), sun azimuth angle, sun altitude angle, and ambient temperature at a certain height are required. These inputs can be obtained from satellite-based data or ground-mounted measurements. However, ground-mounted measurements may have missing data, necessitating pre-processing techniques like data imputation to ensure completeness.

Then, the first loop is created for tilted angles ranging from 0 degrees to 90 degrees with an interval of 1 degrees, but it's observed that angles above 15 degrees show relatively poor power performance in tropical regions. Therefore, the simulation is focused on angles from 0 to 15 degrees to save computation time. The global tilted irradiance is then calculated using the pvlib built-in function for Perez's sky model, especially for the diffuse component of the solar irradiance.

Next, the orientation of the PV system is looped over, represented as the PV azimuth angle ranging from 1 to 360 degrees with the interval of 1°, covering all orientations. This nested looping ensures each azimuth angle runs through the entire set of tilted angles.

After that, the interrow spacing distance is represented by the DL ratio, which is the ratio between interrow spacing and panel length. In this simulation, the panel length is considered as 1 meter. The DL ratio, ranging from 1.0 to 2.0 with intervals of 0.1, is used as the outer loop.

Additionally, a shadow factor is defined for the beam component of solar irradiance due to shading and bypass diodes, resulting in reduced equivalent solar irradiance. A Ross coefficient model is also developed using input data of ambient temperature to estimate the operating temperature of solar cells. The three arrangement studied cases are defined in the simulation, which can be treated as a quadra loop of the simulation.

After summing the three components of tilted irradiance, the global tilted irradiance can be obtained. Running this simulation with loops for tilted angle, orientation, and DL ratio yields corresponding global tilted irradiances under different PV arrangements. Using the MAX built-in function in Python, the maximum global tilted irradiance is looked up. The corresponding tilted angle, orientation, and DL ratio of the maximum global tilted irradiance are identified as the optimal tilted angle, optimal orientation, and optimal DL ratio. The overall procedures are described in Appendix C.

3.5 Analysis of PV System Performance and Optimal Parameters.

The utilization of simulation allows us to input measured data from different locations, which can include satellite-derived or ground-measured databases. Through this simulation, each location can automatically determine not only the highest GTI along with the optimal tilting angle, orientation, and DL ratio of the PV system, but also conduct a thorough investigation into the PV system's performance at that specific location by iterating through various tilting angles, orientations, and DL ratios. Additionally, we will continue to input measured datasets from different locations to obtain the highest GTI with the corresponding optimal parameters at varying latitude angles. Therefore, the analysis can be divided into two main categories: PV system performance analysis at specific locations and the analysis of optimal parameter variations across different latitude angles. Below are the details of these categories:

Location-specific Analysis:

1) The difference between Typical Meteorological Year (TMY) and Time Series (TS) datatypes is investigated.
2) The relationship between the tilted angle and azimuth is explored to optimize the orientation of solar panels for maximum energy absorption based on the site's geographical position.
3) The relation between the global tilted irradiance (GTI) and the DL ratio (the row spacing) is analyzed, further finding the optimum DL ratio.
4) Three different arrangements are considered as case studies: landscape arrangement with four stacked solar panels, linear landscape arrangement with a single solar panel, and portrait arrangement with a single solar panel.

Latitude-based Parameter Analysis:

1) The relation between latitude and the optimal tilted angle of the solar array is analyzed. (A curve fitting function can be built with the coefficients.)

2) The relation between latitude and the optimal azimuth (orientation) of the solar array is analyzed. (A curve fitting function can be built with the coefficients.)

3) The relation between latitude and the optimal DL ratio (row spacing) of the solar array is analyzed.

4) The difference between satellite-derived sources: SolarGis and PVGIS is investigated.

3.5.1 Incorporating Latitude-Based Data into the Simulation

In this stage, the developed model will integrate measured data from various locations with different latitudes into the simulation to determine the respective optimal tilt angles, orientations, and DL ratios. The simulation will provide insight into the influence of geographic location on these optimal parameters, revealing how latitude affects the configuration of photovoltaic (PV) systems.

3.5.2 Comparison of TMY and TS Data from SolarGIS

Next, the simulation will be repeated using two different data types—Typical Meteorological Year (TMY) and Time Series (TS) data—sourced from SolarGIS at the same site. This analysis aims to investigate the relationship between these two data types. The subprogram in Figure 3.6 is explored to extract and calculate the percentage differences between TMY and TS data in terms of optimal parameters. The results will be analyzed in Excel, comparing the DL ratio against the optimal tilt angle, orientation, and Global Tilted Irradiance (GTI) yield. Bar charts will be plotted to highlight any differences between the configurations.

Figure 3.6 shows the flowchart of the subprogram on processing the TS and TMY simulated results.

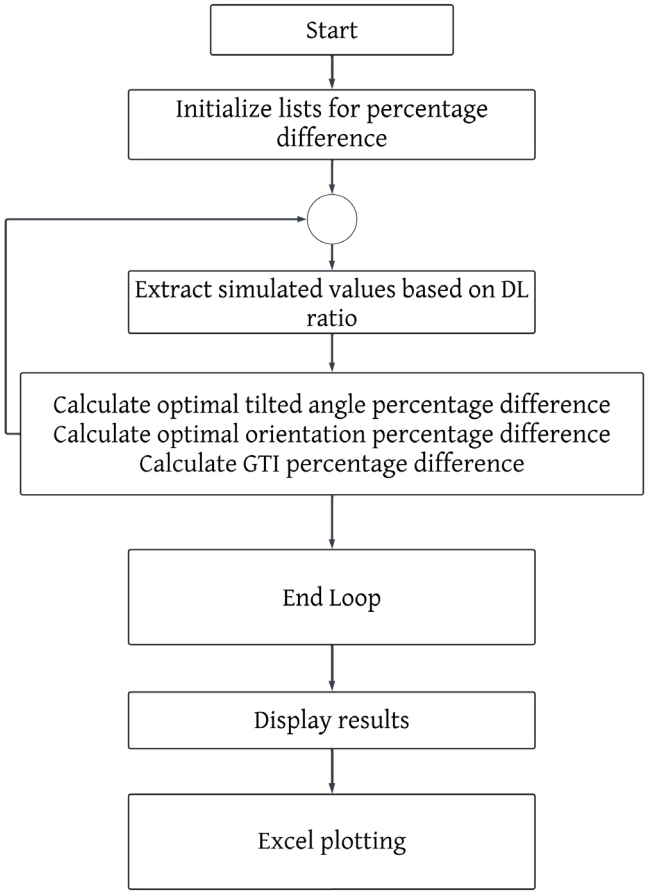

Figure 3.6: Flowchart of TMY and TS data processing.

3.5.3 Correlation Between SolarGIS and PVGIS Databases

A further comparison will be conducted between SolarGIS and PVGIS databases to explore their correlation. A Python program will compile the simulation results as shown in Figure 3.7, which will then be analyzed in Excel to create scatter plots. These plots will investigate relationships between latitude and optimal tilt angle, latitude and optimal orientation, and latitude and highest GTI yield. A final comparison between the simulation results from SolarGIS and PVGIS will also be performed to assess the consistency between the databases.

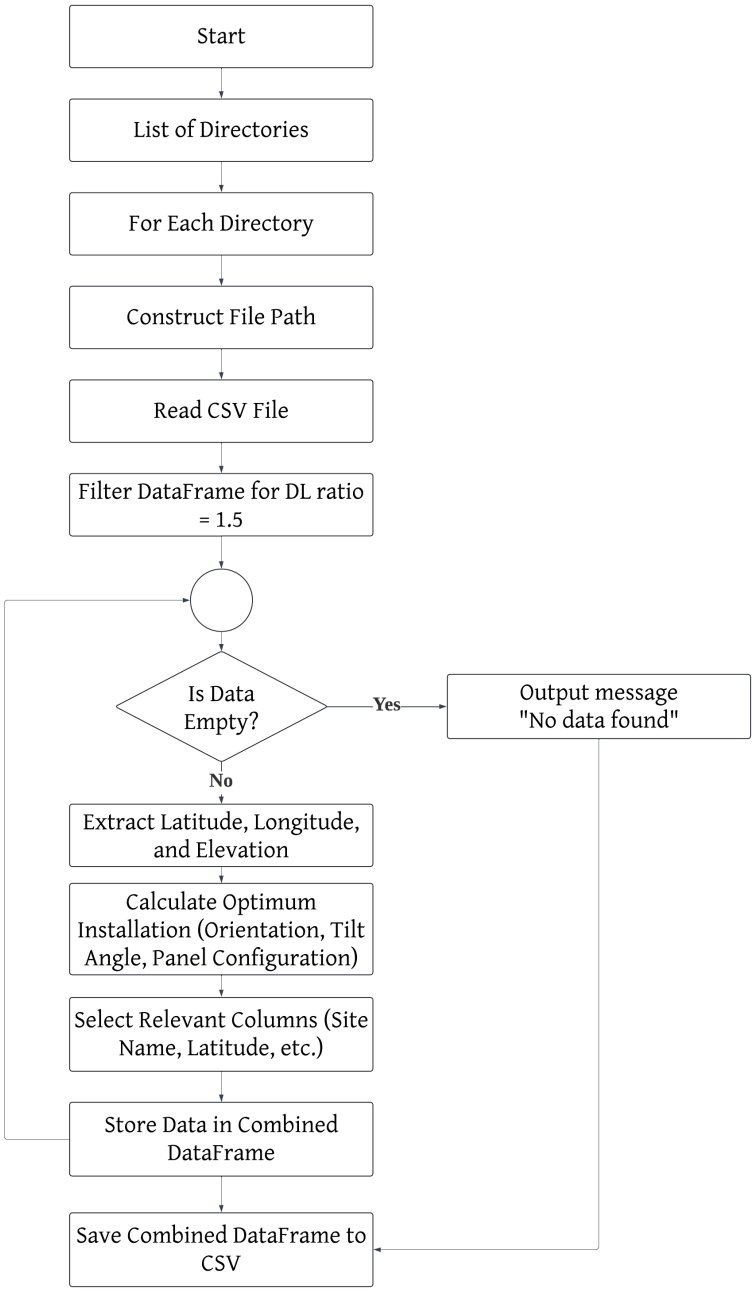

Figure 3.7: Data Filtering and Combination Flowchart for Site Results.

3.5.4 Location-Based Analysis of DL Ratio Response

The simulation results will undergo additional analysis focusing on the response of DL ratios to changes in optimal tilt angles and orientations. A subprogram developed in Python will compile and plot the corresponding analyses for each site. This section shifts from latitude-based to location-based analysis, which

evaluates the specific configuration of PV systems at different sites. The differences between various PV panel configurations will also be explored.

Figure 3.8 captures the core actions of the subcode on processing the location-based analysis.

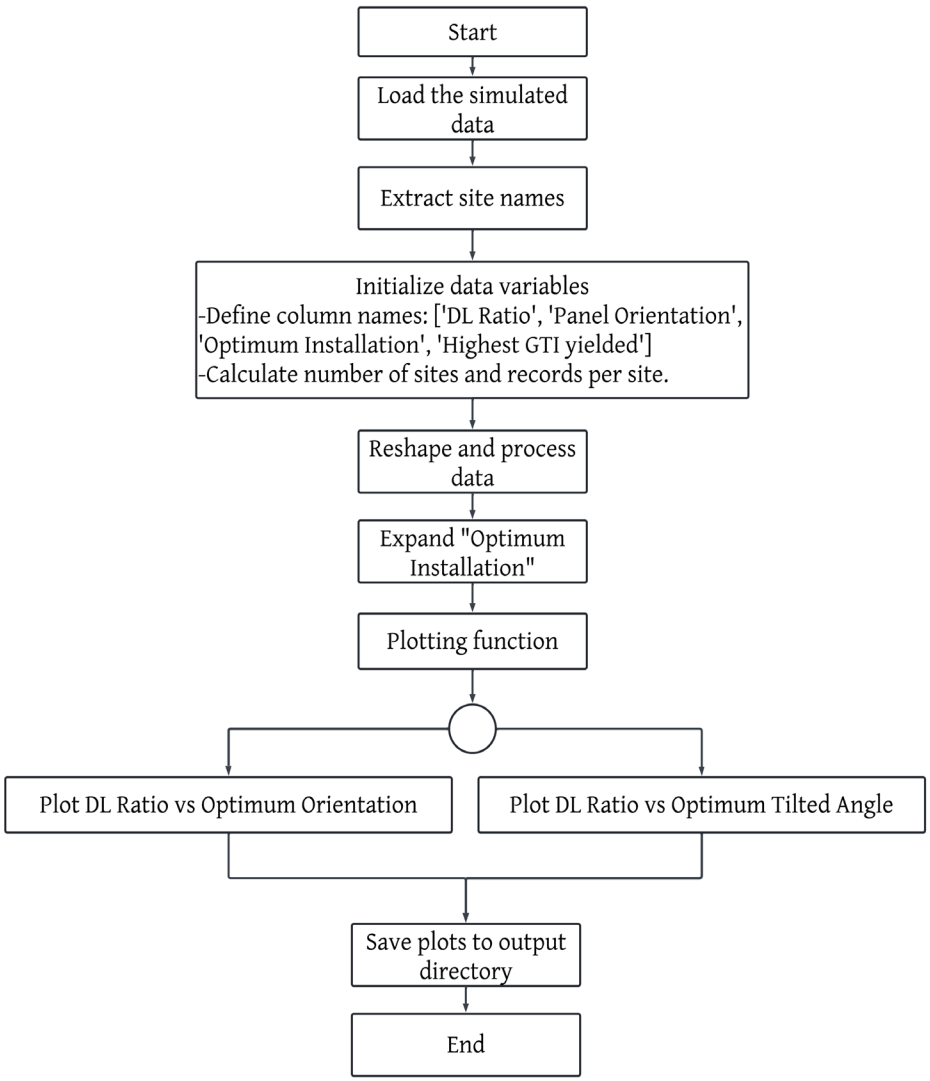

Figure 3.8: Flowchart for Data Processing and Visualization in SolarGis Solar Panel Optimization.

3.5.5 Impact of Tilt and Orientation Variations on GTI Losses

Further analysis will be conducted to assess the impact of small variations in tilt and orientation on GTI losses. A subprogram in Figure 3.9 will extract the GTI yielded at ±3 degrees from the optimal tilt angle and ±30 degrees from the optimal orientation.

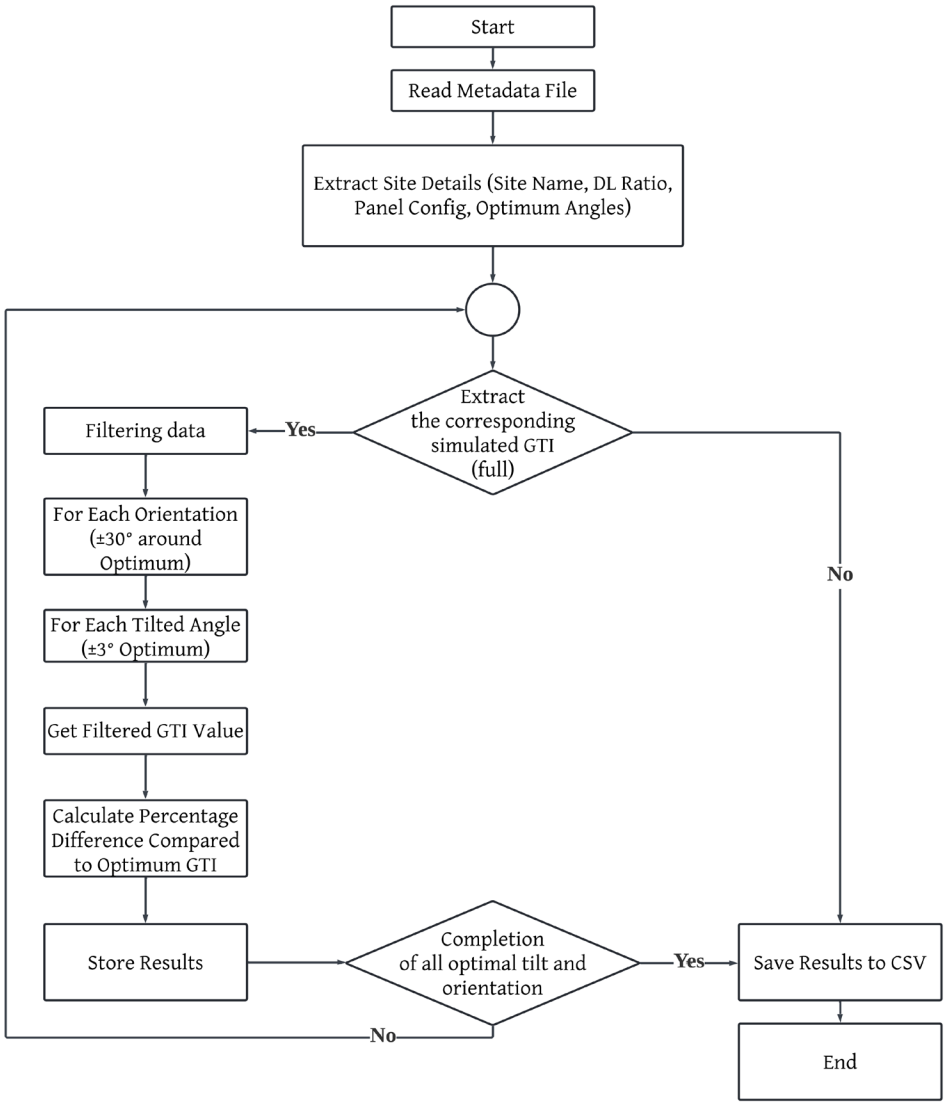

Figure 3.9: Flowchart for GTI data processing under variation of optimal tilted angle and orientation.

The loss percentage between these variations and the highest GTI yield will be calculated using the following Eqn. (3.25):

$$Loss\ Percentage = \frac{|\,GTI_{Highest} - GTI_{\pm 3^\circ\ tilt \backslash \pm 30^\circ}\,|}{GTI_{Highest}} \times 100\% \quad (3.25)$$

3.5.6 Experimental Validation of the Developed Program

To validate the applicability of the developed simulation, experimental data from Goh's setup in 2024 will be referenced as shown in Figure 3.10. The experimental setup consists of eight PV modules arranged in an orthogonal configuration (North, North-East, East, South-East, South, South-West, West, and North-West) with a 10-degree tilt. Data on power output, temperature, and solar irradiance will be collected using APSystems Energy Monitoring and Analysis (EMA) software and a custom-built data logging system.

Figure 3.10: Orthogonal Photovoltaic System Setup. (Goh and Universiti Tunku Abdul Rahman,2024)

The summarized data will be plotted in bar charts to show the received GTI in each direction. The measurement period spans from 15th March 2024 to 14th September 2024, limiting the collection of annual GTI data. To supplement this, satellite-based data for the same period will be used for simulation at the Universiti Tunku Abdul Rahman (UTAR) Sungai Long Campus (3.0396° N, 101.7942° E) in Malaysia. Python code will be utilized to generate counterplots showing variations in the highest GTI yield for different optimal tilt angles and orientations. The comparison between simulated and experimental results will demonstrate the simulation's accuracy and effectiveness. The error percentage between these experimental and simulated GTI yields will be calculated using the following Eqn. (3.26):

$$Error\ Percentage = \frac{|GTI_{Experiemntal} - GTI_{\text{Simualted}}|}{GTI_{Experiemntal}} \times 100\% \quad (3.26)$$

3.6 Flowchart of Work

To summarize the workflow of this project, Figure 3.11 illustrates the overall concept and serves as a guideline for executing the project.

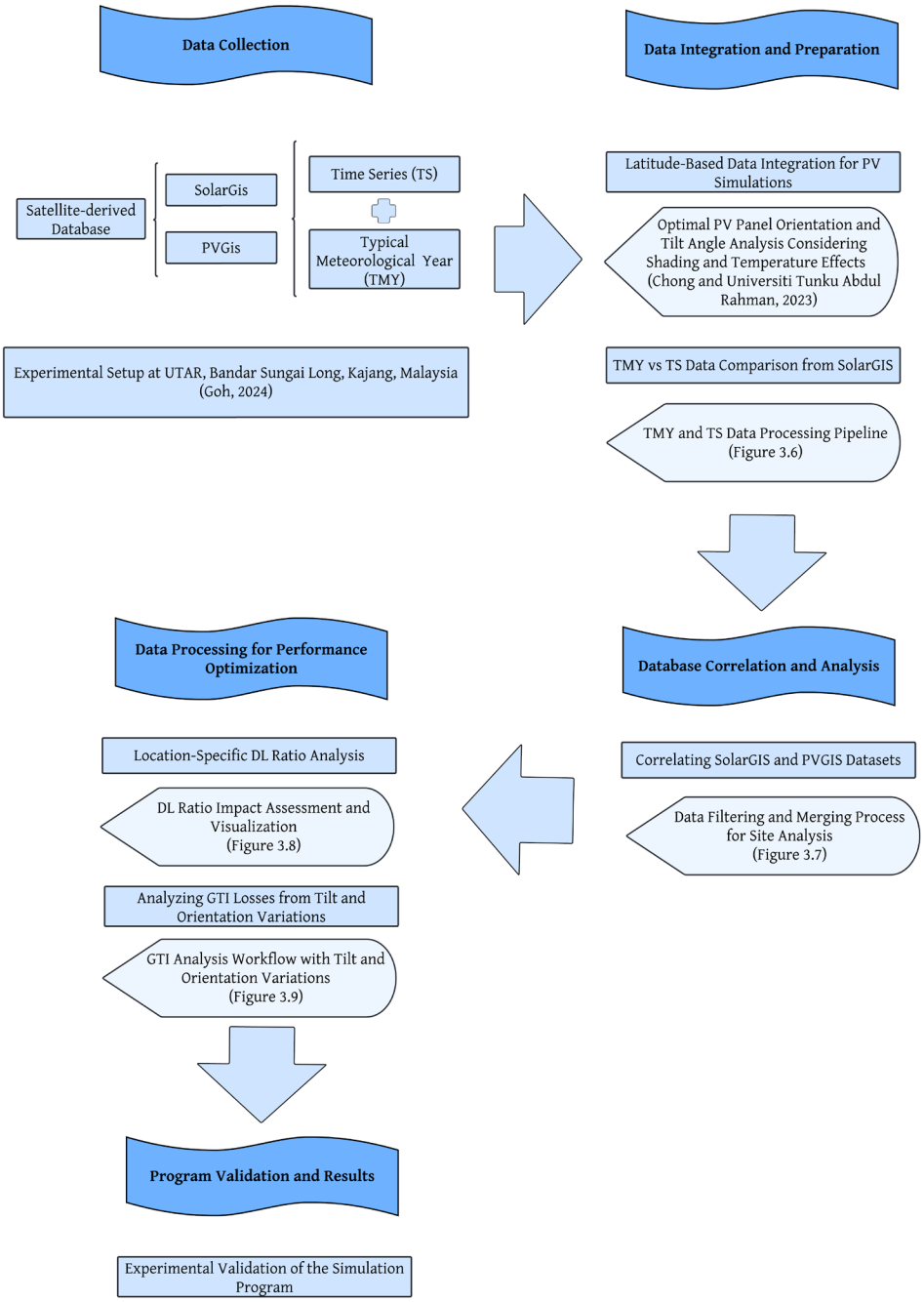

Figure 3.11: Work Flowchart

3.7 Work plan

The work plan of this project is represented in Figure 3.12.

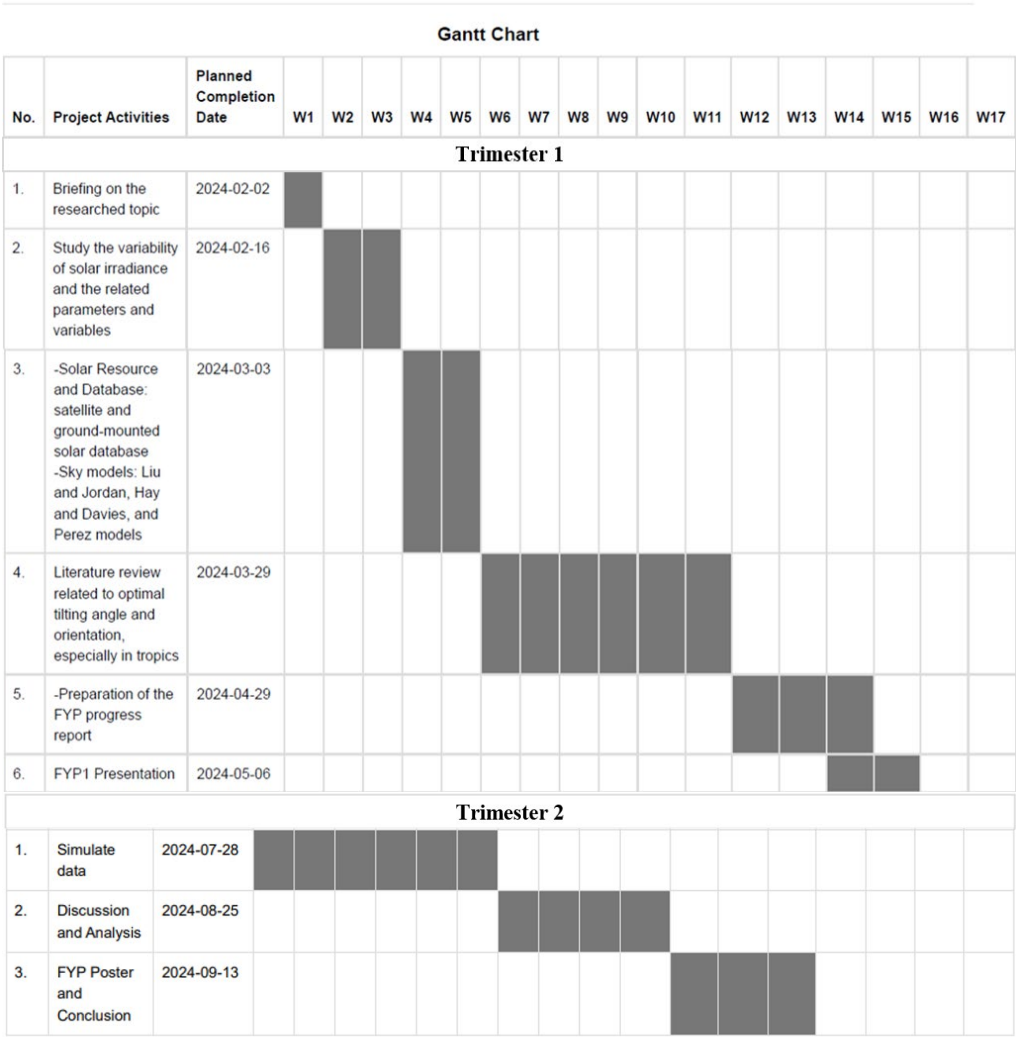

Figure 3.12: Gantt chart for the project.

3.8 Summary

The measured irradiance data from various locations are analyzed using Perez's sky model under tilted conditions of solar panels. This analysis considers variations in tilted angle, orientation, and interrow spacing with three different arrangements of the PV system. Iterative calculations in the simulation are performed to determine the optimal tilted angle, optimal orientation, and optimal DL ratio based on the highest Global Tilted Irradiance (GTI) values. The model incorporates considerations for shading and temperature effects, which significantly influence the overall power performance of the PV system.

CHAPTER 4

RESULTS AND DISCUSSION

4.1 Introduction

This section explores the relationship between latitude and the optimal tilt angle and orientation of photovoltaic (PV) panels in tropical regions, using simulated data from SolarGIS and PVGIS databases as well as the experimental result, as shown in Figure 4.1. It highlights deviations in tilt and orientation due to tropical climate factors like cloud cover and weather patterns, with SolarGIS providing more accurate predictions. The study also examines the impact of DL ratio and panel configurations, finding a DL ratio of 1.5 to be ideal. It compares Typical Meteorological Year (TMY) and Time Series (TS) data, showing minimal differences, and validates its findings with experimental results from Malaysia.

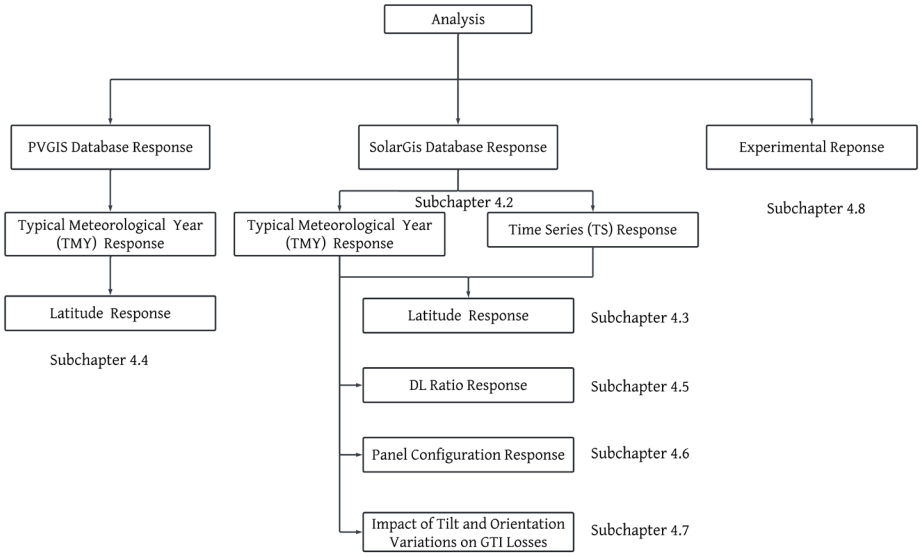

Figure 4.1: Discussion and Analysis Mapping.

4.2 Datatype Response: Typical Meteorological Year (TMY) VS Time Series (TS)

In this section, we discuss the simulated results obtained for West Sumatra, Indonesia (Latitude: 0.10 °N, Longitude: 99.55 °E, Elevation: 4.0 m a.s.l.), Bukit Kemuning Tele Power (Latitude: 2.98 °N, Longitude: 101.51 °E, Elevation: 9.0 m a.s.l.), and Bukit Kayu Hitam Large Scale Solar farm (Latitude:

6.48 °N, Longitude: 100.43 °E, Elevation: 44.0 m a.s.l.) using the Solargis database for TMY and TS data types. The analysis reveals the highest yield of global tilted irradiance (GTI) along with the corresponding optimum tilted angle and orientation. Optimum installations are recorded as (optimum orientation, optimum tilted angle), where optimum orientation denotes the optimal azimuth angle of the PV arrays.

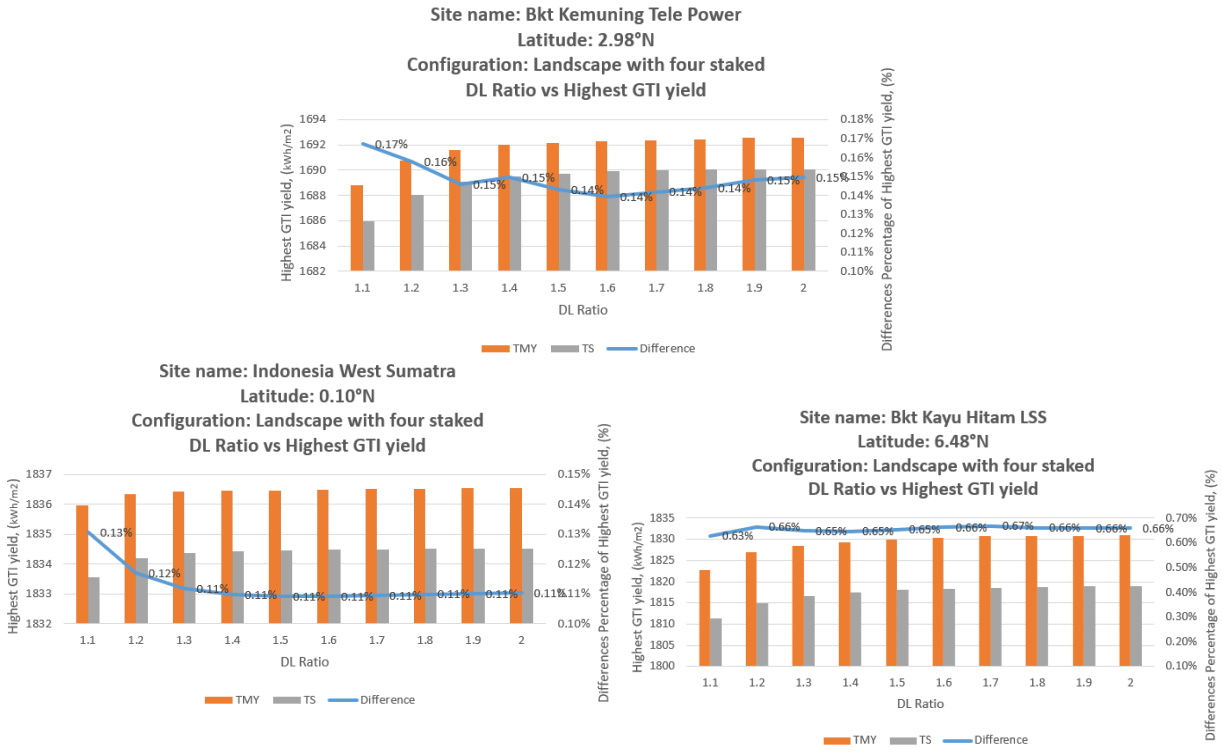

Figure 4.2: Graphs of DL ratio against the highest GTI yielded in three sites: Bkt Kemuning Tele Power in Malaysia (up), West Sumatra in Indonesia (bottom left), and Bkt Kayu Hitam LSS in Malaysia (bottom right).

From Figure 4.2, at West Sumatra, Indonesia, the highest yield GTI values obtained are 1836.55 kW/m² and 1834.53 kW/m² for TMY and TS data, respectively, with the lowest values being 1833.87 kW/m² for TMY and 1100.40 kW/m² for TS data. Comparing these results, the difference in highest yield GTI between TMY and TS data is minimal (approximately 0.1 %), suggesting a similarity that validates their common use.

At Bukit Kemuning Tele Power, the maximum global tilted irradiance (GTI) values recorded are 1692.63 kW/m² for TMY data and 1690.09 kW/m² for TS data, while the minimum values are 1685.31 kW/m² for TMY and 1141.22 kW/m² for TS data. Comparing these figures reveals a minimal difference of approximately 0.15 % in highest yield GTI between TMY and TS data, indicating their comparable suitability for use.

At Bukit Kayu Hitam Large Scale Solar farm, the highest GTI values achieved are 1830.99 kW/m² for TMY data and 1818.99 kW/m² for TS data, with the lowest values at 1811.82 kW/m² for TMY and 1130.33 kW/m² for TS data. Similarly, the difference in highest yield GTI between TMY and TS data is minimal, around 0.6 – 0.7 %, reinforcing their suitability for common applications.

This finding is significant as it can save considerable simulation time. While time series (TS) data offers higher time resolution and potentially more accurate results, it requires significantly more computational time, sometimes orders of magnitude longer, to simulate the same data period and achieve similar outcomes. Therefore, for efficiency in further simulations, TMY data can be effectively utilized with only a slight deviation observed.

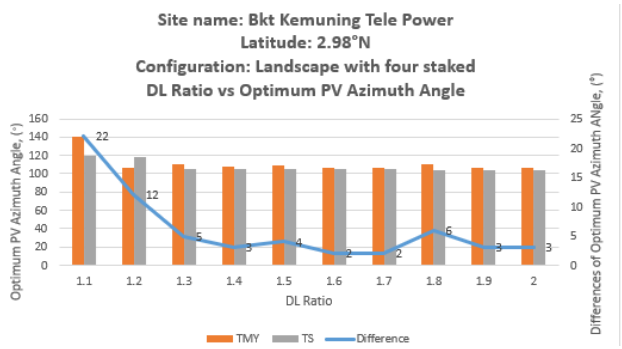

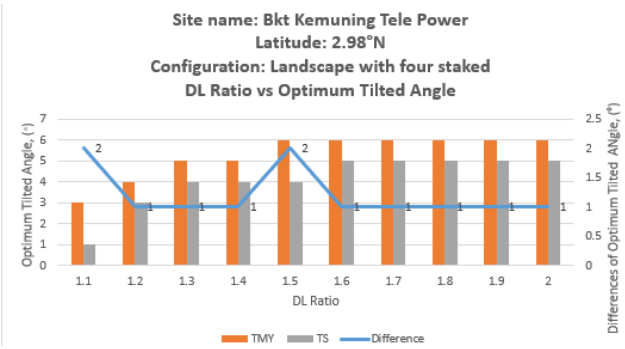

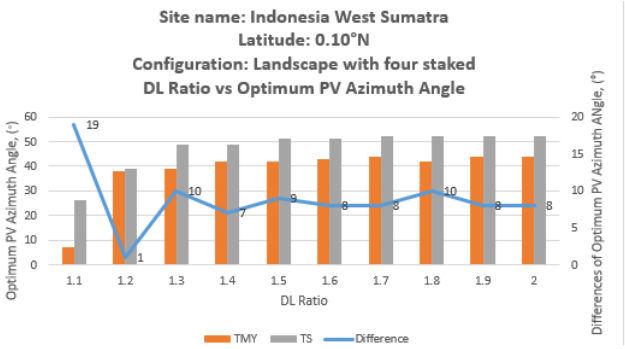

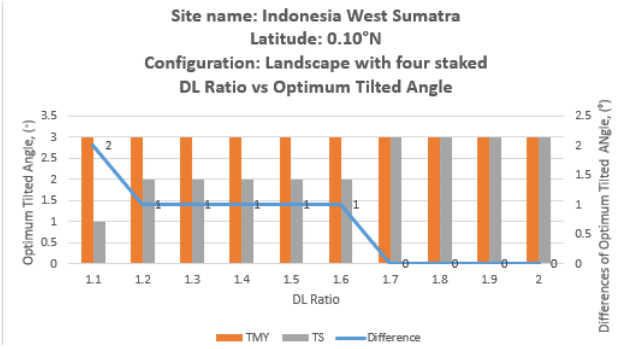

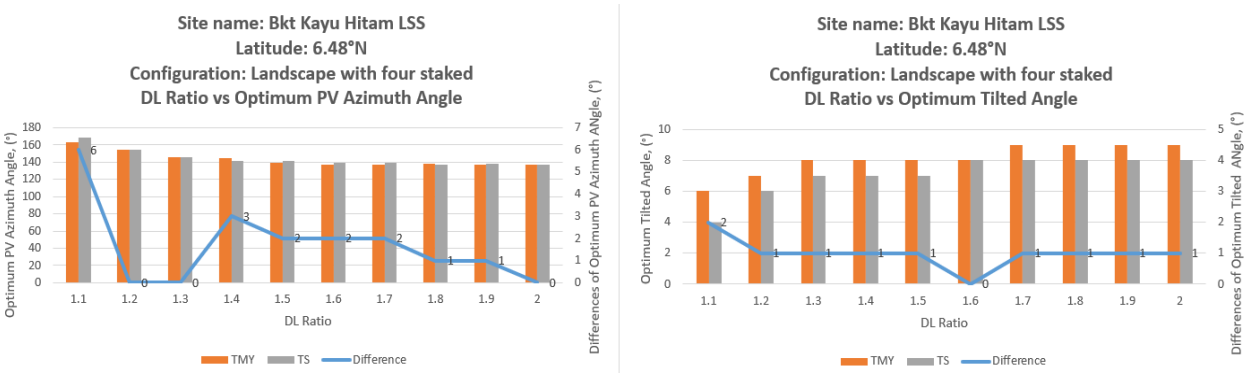

Figure 4.3: Graphs of DL ratio against the optimal tilted angle and optimal orientation in three sites: Bkt Kemuning Tele Power in Malaysia (up), West Sumatra in Indonesia (middle), and Bkt Kayu Hitam LSS in Malaysia (bottom).

Moreover, in Figure 4.3, the optimum tilt angle exhibits a similar trend to the highest yield GTI across different DL ratios. From DL ratio 1.1 to 2.0, the differences in optimum tilt angles between TMY and TS data are consistently small—typically 0, 1, or 2 °—supporting the application of TMY data as the primary simulated data type. However, at DL ratio 1.0, there is a notable fluctuation, likely due to the heightened sensitivity of closely spaced PV systems to the sun's position. This sensitivity can result in significant variations in received solar irradiance, leading to dramatic drops in performance.

Regarding the optimum orientation, the differences between results from the TMY and TS databases are generally within 30 °, with a mode of 8 degrees, which is acceptable for the practical implementation of PV systems. Despite variations between TMY and TS data, all simulated PV orientations consistently indicate that optimal orientations at latitude 0.10 °N tend toward northeast directions. This finding contrasts with the conventional wisdom that optimal orientations should face the equator.

This divergence underscores the importance of site-specific factors, such as local climate and shading considerations, in determining optimal PV orientation, rather than solely relying on latitude-based guidelines. This highlights the research value of our study, particularly in tropical regions where such nuances are critical for maximizing solar energy production.

4.3 SolarGis Database Response

4.3.1 Latitude and Optimal Tilting Angle

Our study focuses on the tropical region, where the relationship between latitude and the optimal tilting angle of photovoltaic (PV) panels has shown distinct trends. As illustrated in Figure 4.4, the simulated data reveal that within the tropical latitudes (10° to 20°), the optimal tilting angle increases with latitude, closely aligning with theoretical models that suggest a linear relationship. Specifically, the optimal tilt angles in this range vary from 10° to 23°, approximately corresponding to the latitude with a deviation of +3 degrees. This correlation aligns with the theoretical expectation that a higher tilt angle is necessary to capture more solar energy due to the lower solar altitude and increased atmospheric path length at higher latitudes.

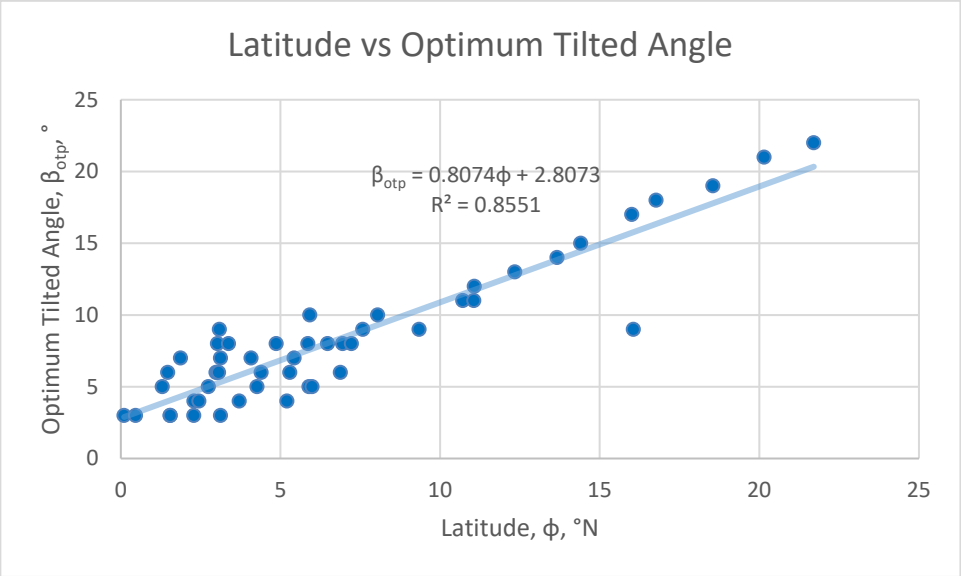

Figure 4.4: SolarGis: Graph of latitude against the optimal tilted angle in the tropical region.

However, the deviations in the optimal tilt angle of photovoltaic (PV) systems become more pronounced at lower latitudes (0° to 10°), where the tilt angle deviates significantly from the latitude, with a spread of ±5 degrees. This increased deviation is largely attributed to tropical climate factors such as highly variable weather conditions, including frequent cloud cover and high humidity. These conditions affect solar irradiance, particularly at noon when solar energy is at its peak but often impeded by cloud cover and precipitation. Additionally,

the high angle of the sun at noon in tropical regions reduces the effectiveness of a fixed tilt angle, leading to greater deviations from the latitude-based optimal tilt.

Graphical analysis supports this observation, showing a wider spread of simulated data points from the trendline in the lower latitude range. The Eqn. 4.1, with an R^2 value of 0.8551 derived from Excel's regression function, describes this trend.

$$\beta_{otp} = 0.8074\,\varphi + 2.8073 \qquad (4.1)$$

The slope of 0.8074 suggests that for each degree increase in latitude, the optimal tilt angle increases by approximately 0.81 degrees, which aligns with theoretical expectations. The intercept of 2.8073 degrees indicates a baseline tilt that accounts for basic tilt requirements independent of latitude.

The resultant Eqn. 4.1 carries a level of uncertainty due to the uneven distribution of sites, primarily concentrated in low-latitude regions. This geographic imbalance introduces potential bias in the model, which may limit its accuracy and reliability when applied to broader latitudinal ranges in the tropics.

However, these findings corroborate previous studies, such as (Mamun, Hasanuzzaman and Selvaraj, 2016), which identified similar trends in tilt angle variation across latitudes. However, this study extends those findings by including a broader range of latitudes and applying more refined data analysis techniques, providing a more detailed understanding of the relationship between latitude and optimal tilt angle.

For PV system designers in tropical regions, these results highlight the importance of customizing the tilt angle to maximize energy yield. In practice, adjustable mounts are recommended for PV systems near the equator, where solar angles and weather conditions vary significantly. At higher latitudes within the tropical zone, a fixed tilt angle near the latitude value may suffice.

4.3.2 Latitude and Optimal Orientation of the PV System

This section examines the relationship between latitude and the optimal orientation of photovoltaic (PV) panels in tropical regions. The orientation of PV panels is critical for maximizing solar energy capture, and it is influenced by the sun's path across the sky, which varies with latitude.

Note that a data point with a negative orientation appears in Figure 4.5. This occurs because the orientation in the plot varies from 0 to 360°, where 180° can equivalently be represented as -180°. However, Excel's built-in functions do not automatically account for this relationship. As a result, the curve-fitting function fails to recognize the equivalence between positive and negative orientations. Consequently, data points in the 270 to 360° (northwest region) are expressed as negative values for optimal orientation.

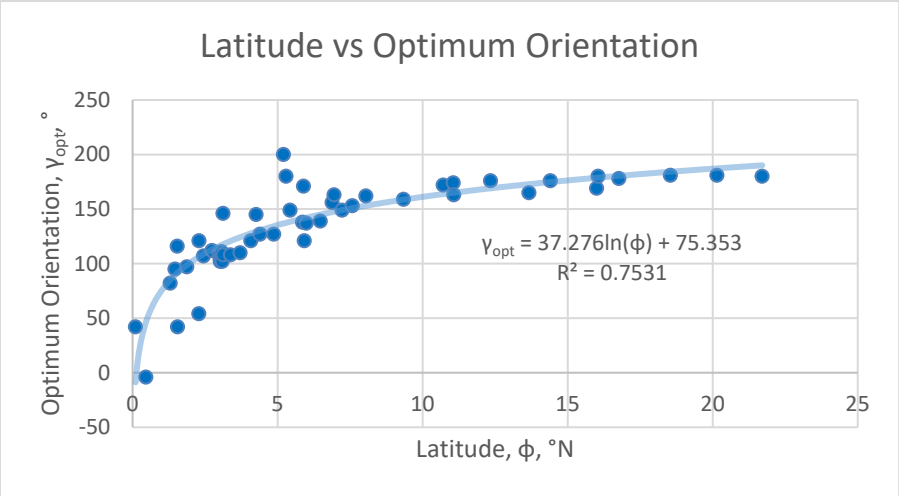

Figure 4.5: SolarGis: Graph of latitude against the optimal orientation in the tropical region.

As illustrated in Figure 4.5, the optimal orientation for PV panels in higher tropical latitudes (10 ° to 20 °) generally favors a direction close to true south (180 °). This is due to the sun's consistent east-to-west movement, with a more pronounced north-south component in high-latitude tropical regions. Near the equator, the sun's path is more vertical, moving almost directly from east to west with higher elevations compared to higher latitudes in the tropical regions. In tropical regions, the minimal seasonal variation results in a stable sun path, making a south-facing orientation effective year-round.

The observed trend aligns with theoretical models, such as those proposed by (Khan et al., 2019), which suggest that a south-facing orientation optimizes solar energy capture in tropical regions due to the sun's high altitude and consistent daily trajectory. The theoretical expectation is thus supported by our results, indicating that a south-facing orientation provides consistent performance.

However, at lower latitudes within the tropical zone (5 ° to 10 °), the optimal orientation tends to shift towards the south-east direction. This shift is more pronounced in regions between 2° and 5°, where the optimal orientation moves towards the east (90 °). At latitudes closer to the equator (0 ° to 2 °), the optimal orientation even approaches the north (0 or 360 °). This variability might be attributed to several factors characteristic of tropical regions, such as frequent weather changes that lead to unstable irradiance and varying solar angles. Additionally, the very high solar angles near the equator can reduce the effectiveness of a strictly south-facing orientation, necessitating adjustments to capture the maximum solar irradiance.

The overall trendline for optimal orientation as a function of latitude can be described by the following equation with an R^2 value of 0.7531.

$$\gamma_{opt}=37.276\ln(\varphi)+75.353 \quad (4.2)$$

The logarithmic nature of the equation suggests a nonlinear relationship between latitude and orientation, especially at low-latitude tropical regions. Specifically, the logarithmic component indicates that as latitude decreases, the rate of change in optimal orientation becomes more pronounced. This reflects the increasing influence of local solar conditions and atmospheric effects as one approaches the equator.

This finding challenges the conventional wisdom of south-facing PV panel orientation, as proposed by Fadaeenejad et al., (2014), which has traditionally been recommended for maximizing solar energy capture with south-facing in northern tropical regions. This shift is attributed to specific characteristics of tropical zones that influence the effectiveness of various panel orientations. In 2022b, Akata et al. emphasized that traditional south-facing panels may not always be the most efficient due to the sun's trajectory, which

requires adjustments to capture solar energy effectively throughout the day, particularly towards the east or southeast at lower latitudes. One significant factor influencing optimal PV panel orientation in the tropics is the high solar elevation angle observed near the equator. During solar noon, the sun's position can be nearly directly overhead. This elevated position reduces the impact of panel orientation on solar irradiance, as the direct sunlight is less sensitive to the directionality of the panels. As a result, the conventional south-facing orientation, which is based on the assumption of a lower solar elevation, becomes less effective in capturing the maximum solar energy. In this context, the deviation observed towards orientations such as southeast or east at lower latitudes can be understood as a response to the high solar elevation angle, where the benefits of a south-facing orientation are diminished.

The experiment of Matius et al. in 2021 also examined key factors influencing the optimal tilt angle and orientation of photovoltaic (PV) systems in tropical regions, with a focus on Malaysia. Given Malaysia's equatorial latitude, the region benefits from high solar radiation levels and relatively constant day lengths, yet optimizing tilt and orientation remains critical for maximizing energy capture. Seasonal variations in the sun's path, though less pronounced than at higher latitudes, necessitate periodic adjustments to the tilt angle to align with the sun's changing position. Monthly variations in the optimal tilt angle, driven by the sun's declination and local weather patterns, further underscore the need for dynamic tilt adjustments to enhance energy output. Local factors such as topography, shading, and wind patterns may require alternative orientations for optimal performance.

For PV system designers, these findings emphasize the importance of orienting PV panels based on latitude to optimize energy capture. In higher latitude tropical regions, panels should be oriented towards true south. In lower latitude regions, orientations may need to adjust from south-east to east, and even north in the closest equatorial regions, to account for the local solar elevation angle, significant azimuth angle variations, minimal seasonal changes, daily solar path characteristics, and local weather patterns. Designing PV systems with adjustable orientations can enhance performance by accommodating these latitude-specific requirements.

4.3.3 Latitude and Highest Yielded GTI of the PV System

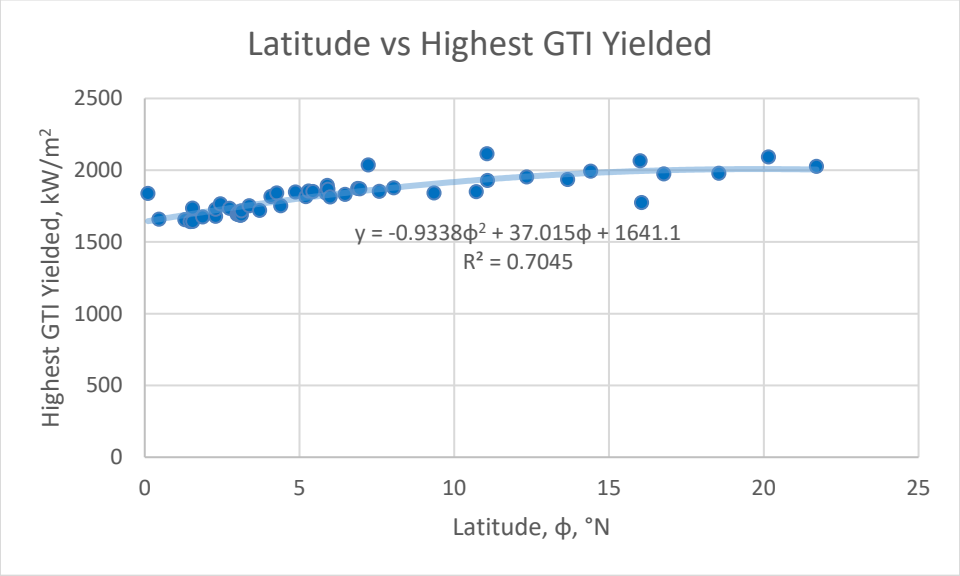

Figure 4.6: SolarGis: Graph of latitude against the highest yielded GTI in the tropical region.

The Global Tilted Irradiance (GTI) is a key performance indicator for photovoltaic (PV) systems, representing the total solar energy captured by the panels. Our analysis reveals a clear relationship between latitude and the highest yielded GTI for PV systems. As illustrated in Figure 4.6, the amount of the highest yielded GTI is generally varied systematically at higher tropical latitudes (around 10° and above). In these regions, the solar angle is more favorable throughout the year due to the sun's consistent path and minimal seasonal variation. This leads to relatively high solar irradiance and a stable GTI, which reaches a saturation point as the tilt angle of the PV panels is optimized to align with the solar path.

At lower latitudes, particularly near the equator, the Global Tilted Irradiance (GTI) is indeed influenced by high solar altitude and consistent solar exposure. However, the decline in GTI efficiency can be attributed to several specific atmospheric and weather-related factors. In tropical regions, sudden weather variations, such as afternoon thunderstorms or cloud cover, are common due to the high temperatures and humidity. This high moisture content leads to rapid vaporization, which results in fast cloud formation, particularly after midday. When cloud cover occurs, it significantly affects the direct

component of sunlight, reducing the total amount of captured irradiance. These frequent weather fluctuations cause greater variability in solar power generation, especially for fixed PV panels that rely heavily on the direct sunlight component. Additionally, a study investigated by Labban and Farahat in 2023 discussed the effects of major dust events in Saudi Arabia, where such environmental factors significantly affect solar irradiance. It found that dust particles in the atmosphere scatter and absorb solar radiation, leading to a reduction in direct and global solar irradiance while increasing the diffuse component. (Labban and Farahat, 2023)

The overall trendline for the highest yielded GTI as a function of latitude can be described by the equation as shown in Eqn. (4.3).

$$y=0.9338\varphi^2+37.015\varphi+1641.1 \quad (4.3)$$

where y represents the highest GTI yielded by the PV system.

This quadratic equation suggests a nonlinear relationship between latitude and GTI. The quadratic term 0.9338x2 indicates that as latitude increases, the effect on GTI becomes more pronounced in a nonlinear manner. The positive coefficient for (37.015) suggests that, initially, GTI increases with latitude, but the rate of increase slows down at higher latitudes. The constant term (1641.1) represents the baseline GTI, which indicates the GTI yield when latitude is zero (theoretically speaking, as a reference point).

For PV system designers, these findings highlight the importance of latitude in optimizing GTI. In higher tropical latitudes, PV systems should be designed to maximize the tilt angle and orientation to achieve high GTI, as the solar exposure is more consistent. In lower latitudes, while GTI remains high, adjustments may be necessary to account for atmospheric effects and the high solar angles. Designing systems with adjustable tilt and orientation can enhance performance by optimizing GTI across varying latitudes.

4.4 PVGIS Database Response

4.4.1 Latitude and Optimal Tilting Angle

In previous section, the simulated results from the Solargis database show a clear, though moderate, linear relationship between latitude and the optimal tilting angle for latitudes ranging from 0° to 20° N. In this section, we will delve into the differences between the results simulated by SolarGis and those from the PVGIS database. Due to time constraints, the number of simulated data points in the PVGIS database is lower, which reduces the accuracy of the regression analysis compared to the data available in the SolarGIS database (11 data points in PVGIS versus 50 in SolarGIS). However, the regression analysis still yielded some interesting results.

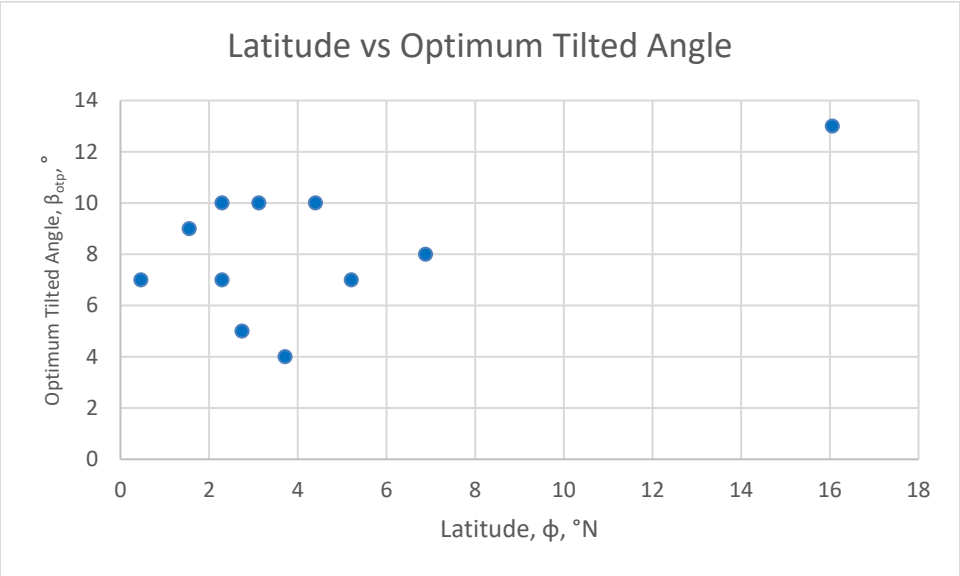

Figure 4.7: PVGIS: Graph of latitude against the optimal tilted angle in the tropical region.

In Figure 4.7, the analysis of PVGIS data shows a roughly linear relationship between latitude and the optimal tilt angle for photovoltaic systems. As latitude increases, the optimal tilt angle gradually rises, with lower latitudes requiring a smaller tilt and higher latitudes necessitating a steeper angle. However, the data exhibit significant variability, particularly in the region near the equator, where other factors such as atmospheric conditions, shading, and local climate appear to play a considerable role in influencing the ideal tilt.

In comparison, SolarGis data shows less variability in tilt angles, particularly at latitudes between 0° and 5°. SolarGis simulations incorporate localized solar irradiance, cloud cover variations, and higher spatial resolution, leading to more accurate tilt angle predictions for near-equatorial regions. Additionally, the increase in optimal tilt angles between 10° and 20° latitude is more gradual in SolarGis compared to PVGIS. SolarGis data also yield higher R^2 values (0.8551), suggesting a stronger correlation between latitude and optimal tilt angle.

In summary, while both PVGIS and SolarGis simulations reveal a positive linear relationship between latitude and optimal tilt angle, SolarGis offers more precise predictions with less deviation at lower latitudes and a more gradual increase at higher latitudes. For PV system design in tropical regions, SolarGis provides more reliable estimates, particularly in locations near the equator.

4.4.2 Latitude and Optimal Orientation of the PV System

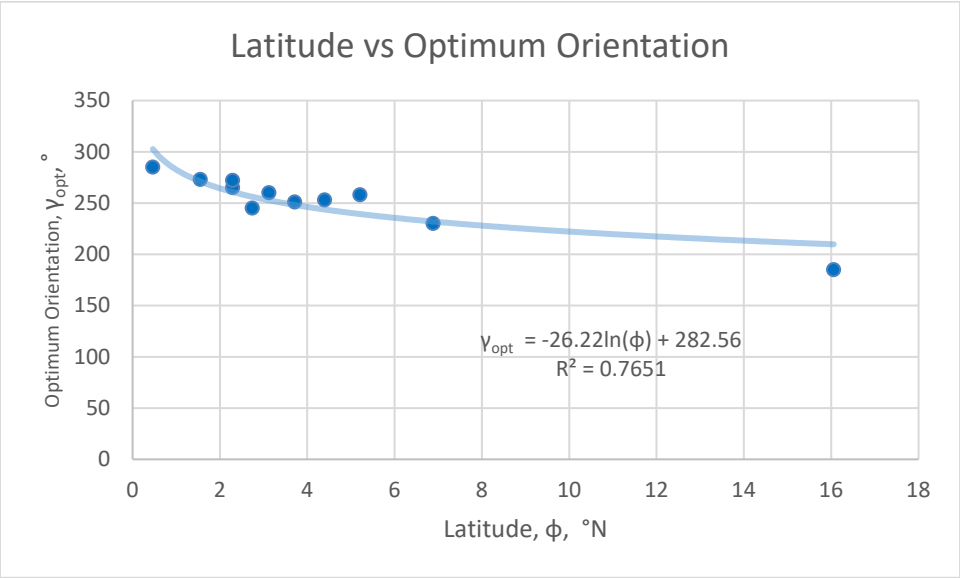

Figure 4.8: PVGIS: Graph of latitude against the optimal orientation in the tropical region.

According to Figure 4.8, the relationship between latitude and the optimal orientation of photovoltaic (PV) systems follows a logarithmic trend, as shown by the PVGIS data in Eqn. (4.4).

$$\gamma_{opt} = -26.22\ln(\varphi) + 282.56 \ (R^2 = 0.7651) \quad (4.4)$$

Eqn. 4.4 illustrates that as latitude increases, the optimal orientation decreases. This logarithmic decay suggests that in tropical regions, the orientation stabilizes at higher latitudes, while at lower latitudes, there is a sharper decline. At very low latitudes (below 2 °N), the optimal orientation shifts from south to southwest and even west, reflecting the need to capture more afternoon sunlight, when solar irradiance is typically higher.

A comparison between PVGIS and SolarGis-derived data reveals distinct differences in how the optimal orientation adjusts with decreasing latitude. PVGIS data show a progression from south to southwest, then west, and eventually north as latitude decreases. This shift highlights the changing position of the sun at lower latitudes and the importance of afternoon solar radiation.

In contrast, SolarGis data indicate a shift from south to southeast, then east, and finally north, emphasizing the morning sun. This shift suggests that SolarGis prioritizes early solar gain, particularly in regions where afternoon cloud cover might reduce solar irradiance. These differing orientation patterns reflect the distinct modeling approaches of the two systems. SolarGis emphasizes early solar capture, while PVGIS focuses on maximizing afternoon radiation.

The primary differences between PVGIS and SolarGis simulations arise from their underlying models and the datasets they use. PVGIS relies on satellite-derived irradiance data and advanced terrain modeling, while SolarGis incorporates higher-resolution data and more advanced modeling techniques, particularly in regions with complex terrain. This may explain the variations in optimal orientation trends, particularly at lower latitudes where terrain and microclimatic effects are more significant.

4.5 DL Ratio Response

4.5.1 DL Ratio and Optimal Tilted Angle of the PV System

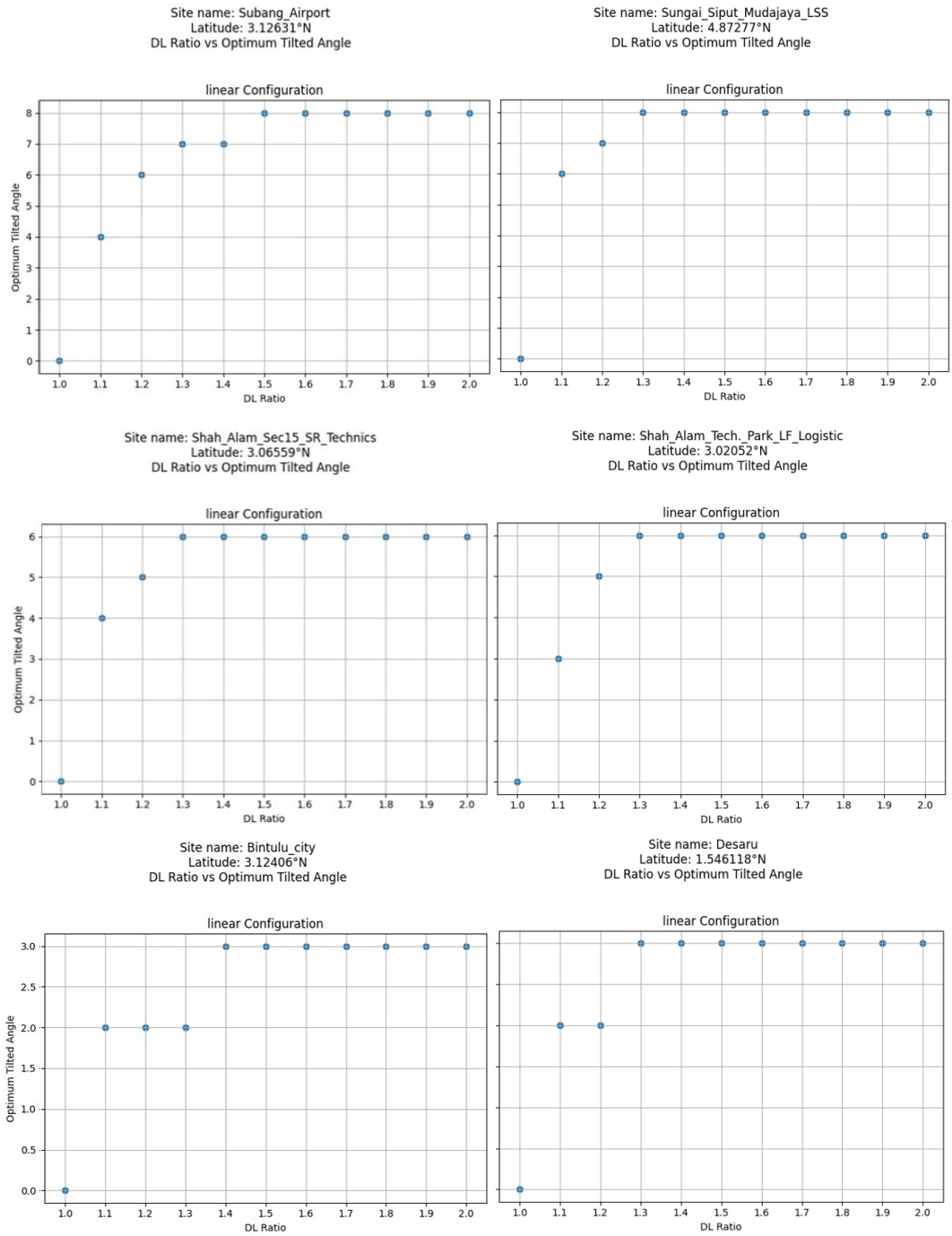

Figure 4.9: Graphs of DL ratio against the optimal tilted angle and optimal orientation in six sites.

The results in Figure 4.9 indicate that once the displacement-length (DL) ratio exceeds 1.5, the optimal tilt angle of the PV system begins to stabilize. At lower DL ratios, the interrow spacing has a pronounced effect on the optimal

tilt angle due to increased shading between rows. As the PV arrays are positioned closer together, the interrow shading effect becomes more significant. Therefore, reducing the tilt angle of the solar panel ensures even sunlight distribution across the panel and reduces the bypass diode effect on the solar panel, leading to the lower optimal tilted angle.

At a DL ratio of 1.5, the optimal tilt angle demonstrates the most consistent performance, suggesting this value is a potential benchmark for PV system designers. This limitation arises because the required shadow length becomes impractically long for one PV panel to shade another, particularly during low sun altitude angles such as those during sunrise and sunset. This ratio reflects the minimum spacing needed to reduce shading while maximizing land usage, a crucial consideration for large-scale solar farm implementations.

One significant finding is the considerable difference in maximum GTI yield between DL ratios of 1.0 and 1.1. This disparity is likely due to the excessively close interrow distance at a DL ratio of 1.0, which amplifies shading effects and diminishes PV performance. The sensitivity of these systems to small variations in solar altitude and azimuth underscores their vulnerability to errors in sunlight distribution. Therefore, they are impractical in real-world applications due to their susceptibility to environmental fluctuations just as the references in the simulation.

Furthermore, the analysis of Figure 4.9 reveals that PV systems in different latitudinal zones can share the same optimal tilt angle at the ideal DL ratio. This phenomenon, particularly evident in Section 4.3.1, highlights the influence of high solar elevation angles and variable weather patterns in tropical regions, resulting in complex, chaotic conditions.

4.5.2 DL Ratio and Optimal Orientation of the PV System

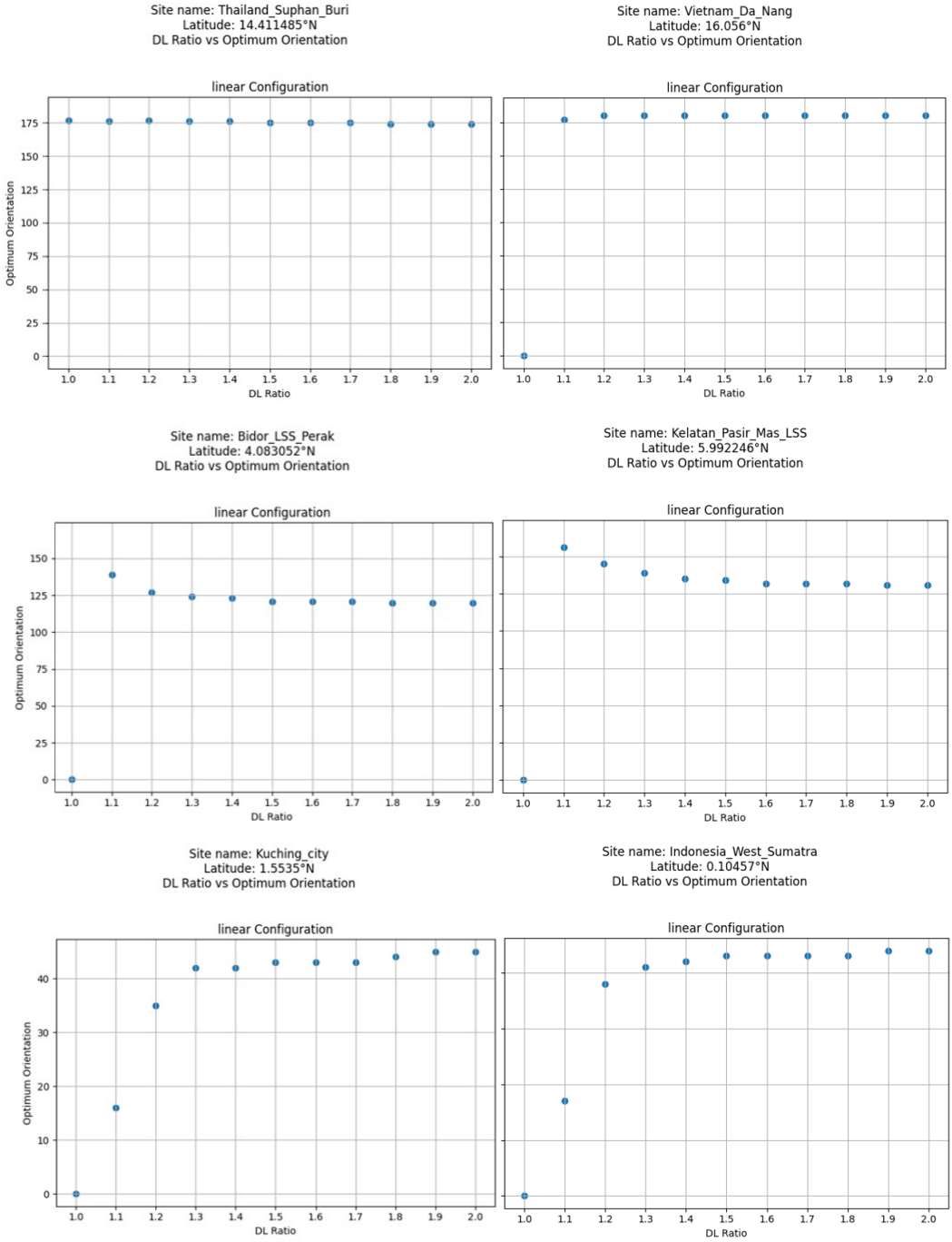

Figure 4.10: Graphs of DL ratio against the optimal orientation in six sites.

The analysis shows that the optimal orientation of photovoltaic (PV) systems follows a similar pattern to the highest yield GTI across different displacement-length (DL) ratios. Above a DL ratio of 1.5, the optimal orientation remains consistent, reinforcing the conclusion that a DL ratio of 1.5 is ideal for tropical regions. This stability arises because the required shadow

length becomes too long for one PV panel to effectively shade the next at higher DL ratios. Below a DL ratio of 1.5, the variation in optimal orientation can manifest in three ways: gradual increase, gradual decrease, or consistency.

Figure 4.10 further illustrates that the type of variation in optimal orientation correlates with latitude. At low latitudes, around 1°N, optimal orientation tends to gradually increase due to the high sun elevation, which distributes sunlight more evenly. This results in a tendency toward a horizontal placement, as tilted surfaces do not significantly increase solar energy capture. Simulated results indicate that PV panels in these regions may even face north. In mid-latitudes, around 5°N, optimal orientation shifts from south to southeast or east as the DL ratio increases from 1.1 to 1.5. At higher tropical latitudes (above 10°N), the optimal orientation is reached at smaller interrow spacing, suggesting that interrow shading effects are less significant for the variation of the orientation in these regions.

Figure 4.10 also partially demonstrates the trend of optimal orientation with latitude variation at the optimal DL ratio of 1.5. Specifically, at higher tropical latitudes, PV systems tend to face south to capture the maximum GTI. As latitude decreases, the optimal orientation shifts gradually towards the southeast, east, and even north. This observation supports the phenomena discussed in Section 4.3.2, highlighting the complex interplay between latitude, DL ratio, and solar orientation in tropical regions.

4.6 Panel Configuration Response: Linear Landscape VS Four Stacked-Panels Landscape VS Portrait

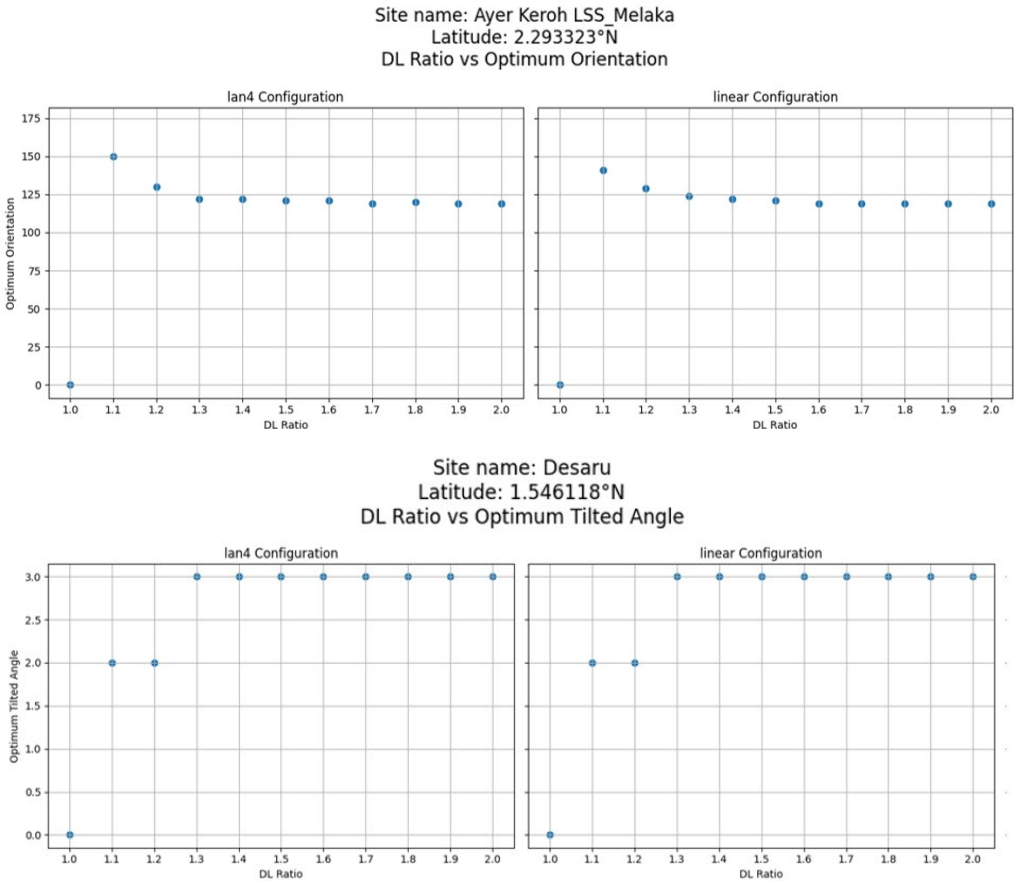

Figure 4.11: Graphs of DL ratio against the optimal tilted angle and optimal orientation of the linear landscape configuration with single-row solar panels and rows of stacked solar panels in different sites.

In evaluating the impact of solar panel configurations on optimal parameters such as tilt angle, orientation, and DL ratio, it is observed that variations between linear landscape and landscape configurations with four-stacked-panels setups have minimal effects in Figure 4.11 no matter at which location. The fundamental difference between these configurations lies in the number of solar panels stacked on the support structure. Despite this variation, the internal circuit configuration of the panels remains consistent across different setups. Therefore, changes in the quantity of stacked PV panels or bypass diodes do not significantly influence the optimal parameters for these configurations.

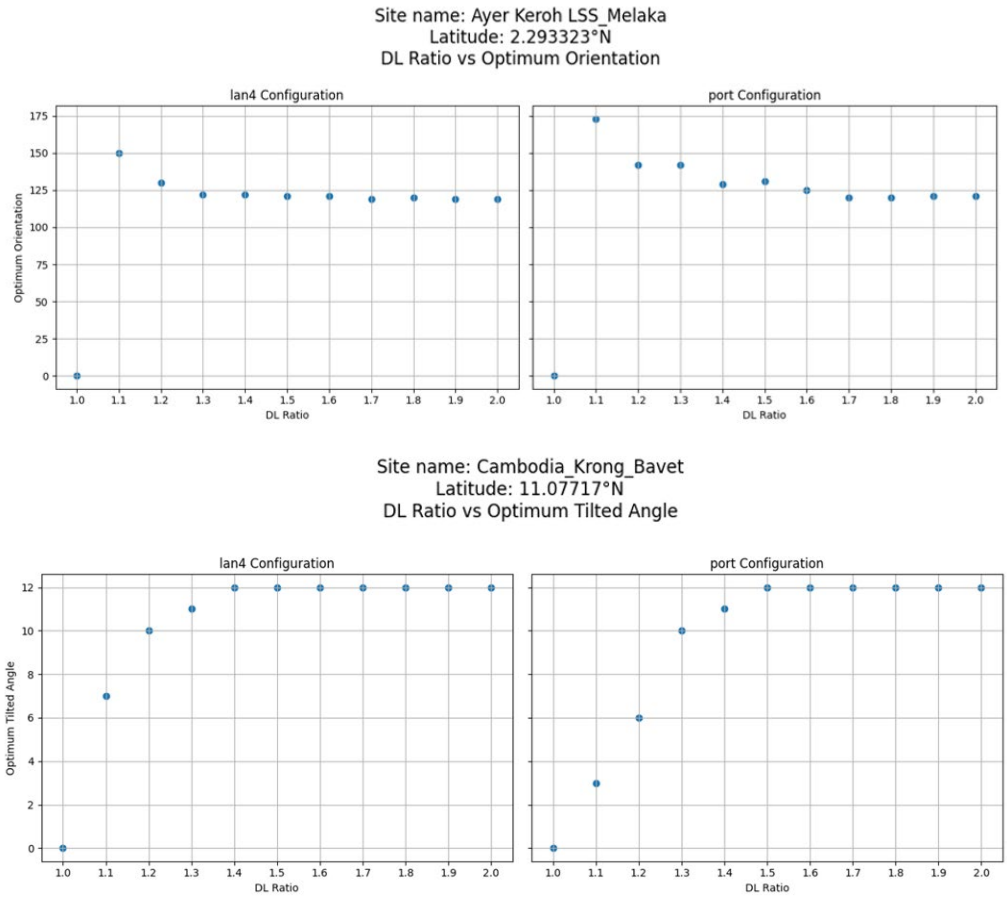

Figure 4.12: Graphs of DL ratio against the optimal tilted angle and optimal orientation of the landscape configuration with four rows of stacked solar panels and portrait configuration with single-row solar panels in different sites.

In Figure 4.12, a more pronounced difference is evident when comparing landscape and portrait orientations of solar panels. Specifically, portrait configurations generally necessitate a higher DL ratio to maintain consistent optimal tilt angles and orientations. This requirement is driven by solar panels oriented in portrait mode are more susceptible to power loss when partially shaded, particularly along the bottom row of cells. This increased susceptibility occurs because shading in this orientation causes the entire panel to behave as though it were fully shaded, resulting in a substantial reduction in energy output. (Oufettoul et al., 2023)

Conversely, solar panels mounted in landscape orientation demonstrate greater resilience to shading. When shading affects the bottom row of cells in

this configuration, the reduction in overall power output is less severe compared to the portrait orientation. This improved performance is attributed to the arrangement of cell subparts within the panel and the function of bypass diodes. For example, in landscape mode, shading one subpart of the panel typically results in a power loss of approximately one-third, while shading two subparts causes a two-thirds loss. This is because the unshaded subparts continue to operate effectively, thereby reducing the overall impact of shading. In contrast, shading the bottom part of the portrait configuration particularly results in turning off the whole solar panel. (Chepp and Krenzinger, 2021)

4.7 Impact of Tilt and Orientation Variations on GTI Losses

This section provides an analysis of the impact of tilt angle and orientation on Global Tilted Irradiance (GTI) loss percentages, based on the analysis of multiple sites. The findings are visualized in Figure 4.13, which demonstrates that nearly all locations experience GTI losses of less than 1% when the tilt angle deviates by ±3 degrees or when the orientation shifts by ±30 degrees.

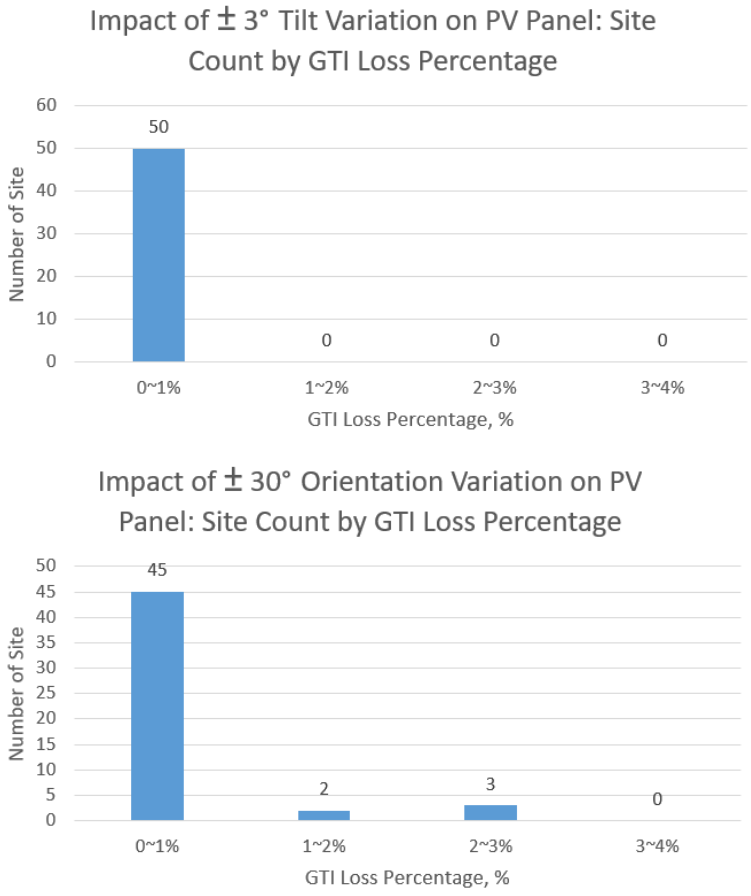

Figure 4.13: Graphs of the site count according to the corresponding GTI losses with optimal tilt angle deviations of ±3 ° (up) and orientation shifts of ±30 ° (bottom) in tropical regions.

These results highlight that minor variations in tilt angle and orientation have a negligible effect on energy production efficiency. Consequently, PV system designers do not need to adhere to overly strict precision standards for tilt angle and orientation during installation. This relaxation in precision requirements suggests that installation costs can be reduced, as the need for specialized equipment or labor to achieve highly accurate angles is minimized without significantly affecting performance.

Overall, this analysis supports the notion that the cost associated with the installation of PV systems can be lowered without compromising energy output, making the system more economically feasible while maintaining performance reliability.

4.8 Experimental Results of Tilt and Orientation on GTI yielded

In this section, we compare the simulated results with the experimental data collected from the system established by Goh in 2024. The experimental setup commenced operation on March 15, 2024, with the final measurements recorded on September 13, 2024. To ensure a thorough comparison, the simulation was conducted for the same period using satellite-derived data from the SolarGis database, specifically focusing on Typical Meteorological Year (TMY) data for the corresponding location. The simulation was designed to match the experimental setup in terms of location and non-shading effect conditions.

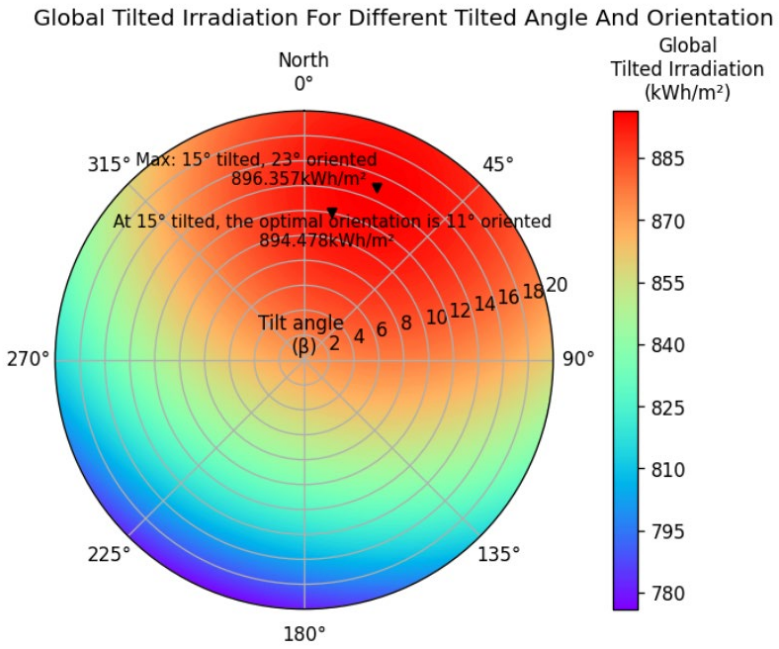

Figure 4.14: Counter plot of GTI at different tilted angles and orientations in Bandar Sungai Long.

Based on the contour plot in Figure 4.14, the analysis shows that for the period between March and September in Bandar Sungai Long, Malaysia, the optimal direction for a solar PV system is a 23° shift from true north towards the east, with a recommended tilt angle of 15°. This configuration yielded a Global Tilted Irradiance of 896.537 kW/m² within this period. Meanwhile, at the fixed tilted angle of 10°, the corresponding optimal orientation is 11° shift from true north towards the east and the resultant GTI is 894.478 kW/m². In Malaysia, particularly from March to September, the sun shifts towards the northern hemisphere, making a north-facing orientation ideal for maximizing sunlight exposure. During this period, the sun's path relative to the equator allows PV systems with a slight eastward shift to capture the most sunlight, especially around the equinoxes in March and September when the sun is directly overhead. This setup optimizes the solar gain and enhances the energy yield of the system. (Billy, 2017)

While the simulation indicates the optimal orientation and tilt angle for maximum energy production, it is important to note that between October and February, the sun moves to the southern hemisphere. However, due to

Malaysia's proximity to the equator, this shift is less pronounced, and a north-facing orientation remains effective for most of the year. (Billy, 2017)

In the experimental setup, it was not feasible to implement a wide range of tilt angles (0 to 20 °) and orientations (0 to 360 ° at 1-degree intervals) due to cost and time constraints. Instead, the practical setup tested a fixed tilt angle of 10 ° and eight discrete orientations: true north, northwest, west, southwest, south, southeast, east, and northeast, arranged in an orthogonal shape.

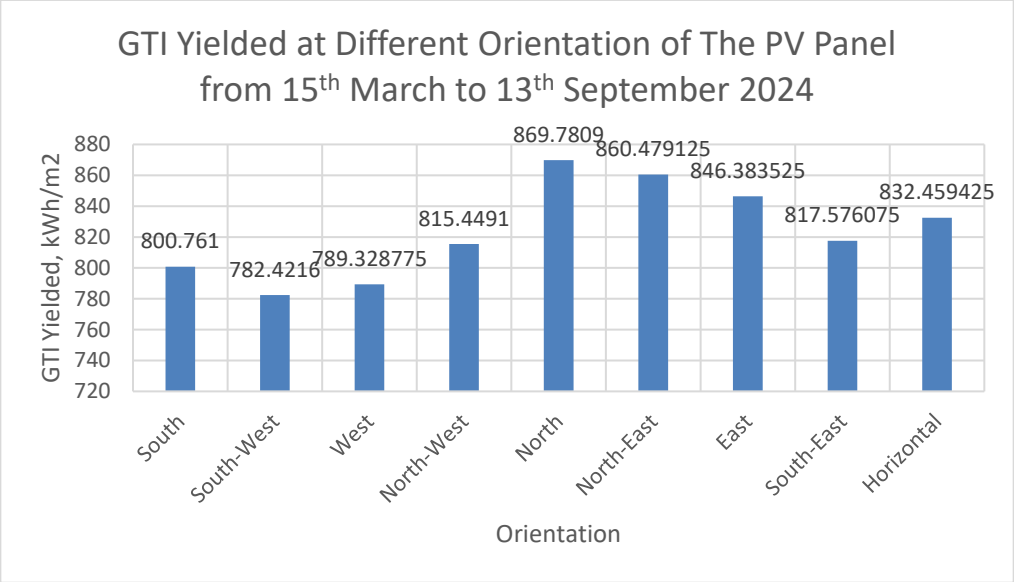

Figure 4.15: Graph of the experimental yielded GTI at different orientations from March to September on the rooftop of UTAR in Bandar Sungai Long.

Despite the limitations, the results as shown in Figure 4.15 indicate that the best orientation for the installed PV system aligns closely with the simulated results, favoring a direction of true north. The measured GTI in this orientation was 869.7809 kWh/m^2, which was higher than in other tested directions, corroborating the simulation's prediction of optimal performance near the northern direction. While the experimental results do not fully explain the observed shift in optimal orientation typically associated with lower tropical latitudes throughout a year as shown in Section 4.3.2, they provide sufficient evidence to validate the accuracy of the simulation in estimating the optimal parameters for the PV system.

To further demonstrate the accuracy of the developed simulation, the corresponding error percentages were calculated and are summarized in Table 4.1.

Table 4.1: Error percentage summary for the developed simulation on GTI.

Orientation	Global Tilted Irradiance (kWh/m^2)		Error Percentage
	Real PV System	Simulated Result	
South	800.76	835.52	4.34%
South-West	782.42	835.95	6.84%
West	789.33	852.30	7.98%
North-West	815.45	874.62	7.26%
North	869.78	891.00	2.44%
North-East	860.48	891.28	3.58%
East	846.38	875.14	3.40%
South-East	817.58	852.05	4.22%
Horizontal	832.46	870.66	4.59%

The error percentages in each direction are less than 10%, indicating a high level of accuracy in the developed simulation. This low margin of error suggests that the simulation reliably captures the expected outcomes across different orientations or variables. The consistency of the error values across all directions further reinforces the robustness of the model, making it a suitable tool for predicting and analyzing real-world scenarios within an acceptable range of uncertainty. These results validate the simulation's performance and enhance its credibility for discussions in this chapter and future applications.

4.9 Summary

In a nutshell, this chapter analyzes the impact of latitude, DL ratio, and panel configuration on the optimal tilt angle and orientation of PV systems in tropical regions. It finds that the optimal tilt angle generally increases with latitude, while the optimal orientation shifts from south to southeast and east as latitude decreases. A DL ratio of 1.5 is found to be ideal for consistent performance. Additionally, the chapter compares simulated data with experimental results from Malaysia, validating the simulation's accuracy in predicting optimal parameters.

CHAPTER 5

CONCLUSIONS AND RECOMMENDATIONS

5.1 Conclusion

This project investigated the optimal tilt angle and orientation for photovoltaic (PV) systems in tropical regions, analyzing the impact of latitude, interrow spacing (DL ratio), and panel configuration on energy yield. The study relied on simulated data from SolarGIS and PVGIS databases with different datatypes of Typical Meteorological Year (TMY) and Time Series (TS), supplemented by experimental validation from Malaysia.

The findings revealed that optimal tilt angles generally increase with latitude, aligning with theoretical models, but deviating at lower latitudes likely due to tropical climate factors. Optimal orientation shifted from south to southeast and east as latitude decreased, emphasizing the need for site-specific adjustments in the tropics. This observation challenges the conventional wisdom of south-facing panels being universally ideal. A DL ratio of 1.5 was identified as optimal for consistent performance, balancing interrow shading with land usage. Additionally, the minimal deviation between TMY and TS simulations from SolarGIS suggests their interchangeable and universal use for PV system performance analysis. The study also found that variations in tilt (±3°) and orientation (±30°) have minimal impact on energy output, providing flexibility in installation practices.

The simulation's accuracy was validated through comparison with experimental data from Universiti Tunku Abdul Rahman, Bandar Sungai Long, Malaysia, showing consistent optimal orientation predictions. However, the experimental setup's limitations prevented a full exploration of the optimal tilt angle range.

5.2 Recommendations for Future Work

To provide insights into areas that could benefit from further research and development to enhance the understanding and performance of PV systems, this section outlines the recommendations for future work based on the findings of this study:

1. Expand Experimental Validation: Conduct experiments with a wider range of tilt angles and orientations to fully validate the simulation findings across diverse tropical conditions.
2. Investigate Specific Tropical Weather Effects: Analyze the impact of cloud cover patterns, rainfall, and humidity on optimal PV system parameters in different tropical regions.
3. Incorporate Advanced Shading Scenarios: Model and analyze more complex shading situations, including partial shading from nearby structures or vegetation, to improve real-world applicability

REFERENCES

Ångström, A., 1924. Solar and terrestrial radiation. Report to the international commission for solar research on actinometric investigations of solar and atmospheric radiation. *Quarterly Journal of the Royal Meteorological Society*, [online] 50(210), pp.121–126. https://doi.org/10.1002/qj.49705021008.

Asl-Soleimani, E., Farhangi, S. and Zabihi, M., 2001. The effect of tilt angle, air pollution on performance of photovoltaic systems in Tehran. *Renewable Energy*, [online] 24(3–4), pp.459–468. https://doi.org/10.1016/s0960-1481(01)00029-5.

Beckman, O., 1997. *Ångström, father and son*. S. Academiae Ubsaliensis.

Billy, 2017. *Going Solar Chapter 4: Know where to face your solar PV panels*. [online] Green Sarawak. Available at: <https://greensarawak.com/things-to-know-before-going-solar/going-solar-chapter-4-know-where-to-face-your-solar-pv-panels/>.

Cebecauer, T. and Šúri, M., 2016. Site-adaptation of satellite-based DNI and GHI time series: Overview and SolarGIS approach. *AIP Conference Proceedings*. [online] https://doi.org/10.1063/1.4949234.

Chepp, E.D. and Krenzinger, A., 2021. A methodology for prediction and assessment of shading on PV systems. *Solar Energy*, [online] 216, pp.537–550. https://doi.org/10.1016/j.solener.2021.01.002.

Chong, B.Y. and Universiti Tunku Abdul Rahman, 2023. *OPTIMAL ORIENTATION AND TILTING ANGLE OF PV PANELS CONSIDERING SHADING AND TEMPERATURE EFFECTS*. [online] *UTAR Institutional Repository*. Available at: <http://eprints.utar.edu.my/5644/1/3E_1803849_FYP_report_-_BOON_YOONG_CHONG.pdf>.

Duffie, J.A. and Beckman, W.A., 2013b. *Solar engineering of thermal processes*. [online] https://doi.org/10.1002/9781118671603.

Elsayed, M.M., 1989b. Optimum orientation of absorber plates. *Solar Energy*, [online] 42(2), pp.89–102. https://doi.org/10.1016/0038-092x(89)90136-9.

Fadaeenejad, M., Radzi, M.A.M., Fadaeenejad, M., Zarif, M. and Gandomi, Z., 2014. Optimization and comparison analysis for application of PV panels in three villages. Energy Science & Engineering, [online] 3(2), pp.145–152. https://doi.org/10.1002/ese3.52.

Fedkin, M., A., J., Dutton e-Education Institute, College of Earth and Mineral Sciences, and Penn State University, 2024. *3.3. Cosine Effect | EME 812: Utility Solar Power and Concentration*. [online] Available at: <https://www.e-education.psu.edu/eme812/node/896> [Accessed 23 April 2024].

Friesen, G., Pavanello, D. and Virtuani, A., 2010. Overview of Temperature Coefficients of Different Thin Film Photovoltaic Technologies. *25th European Photovoltaic Solar Energy Conference and Exhibition*, [online] pp.4248–4252. https://doi.org/10.4229/25theupvsec2010-4av.3.83.

George, A.A. and Anto, R., 2012. Analytical and experimental analysis of optimal tilt angle of solar photovoltaic systems. *2012 International Conference on Green Technologies (ICGT)*. [online] https://doi.org/10.1109/icgt.2012.6477978.

Hay, J.E., 1979. Calculation of monthly mean solar radiation for horizontal and inclined surfaces. *Solar Energy*, [online] 23(4), pp.301–307. https://doi.org/10.1016/0038-092x(79)90123-3.

Hottel, H.C. and Woertz, B.B., 1942. The performance of Flat-Plate Solar-Heat collectors. *Transactions of the American Society of Mechanical Engineers*, [online] 64(2), pp.91–103. https://doi.org/10.1115/1.4018980.

Iqbal, M., 1983. *An introduction to solar radiation*. [online] *Elsevier eBooks*. https://doi.org/10.1016/b978-0-12-373750-2.x5001-0.

Ismail, D., Irwanto, M., Irwan, Y.M., Gomesh, N. and Ahmad, N.S., 2011. Clear sky global solar irradiance on tilt angles of photovoltaic module in Perlis, Northern Malaysia. *International Conference on Electrical, Control and Computer Engineering 2011 (InECCE)*. [online] https://doi.org/10.1109/inecce.2011.5953923.

Khan, T.M.Y., Soudagar, M.Elahi.M., Kanchan, M., Afzal, A., Banapurmath, Nagaraj.R., Akram, N., Mane, S.D. and Shahapurkar, K., 2019. Optimum location and influence of tilt angle on performance of solar PV panels. *Journal of Thermal Analysis and Calorimetry*, [online] 141(1), pp.511–532. https://doi.org/10.1007/s10973-019-09089-5.

Khatib, T., Mohamed, A.B. and Sopian, K., 2012b. On the monthly optimum tilt angle of solar panel for five sites in Malaysia. *2012 IEEE International Power Engineering and Optimization Conference Melaka, Malaysia*. [online] https://doi.org/10.1109/peoco.2012.6230827.

Klucher, T.M., 1979. Evaluation of models to predict insolation on tilted surfaces. *Solar Energy*, [online] 23(2), pp.111–114. https://doi.org/10.1016/0038-092x(79)90110-5.

Labban, A. and Farahat, A., 2023. Effect of Major Dust Events on Ambient Temperature and Solar Irradiance Components over Saudi Arabia. *Atmosphere*, [online] 14(2), p.408. https://doi.org/10.3390/atmos14020408.

Levitskiy, M., 2023. *Renewable energy challenges in 2024 and how custom software can help*. [online] Blog. Available at: <https://tech-stack.com/blog/custom-software-challenges-renewable-energy/>.

Liu, B.Y.H. and Jordan, R., 1960. The interrelationship and characteristic distribution of direct, diffuse and total solar radiation. *Solar Energy*, [online] 4(3), pp.1–19. https://doi.org/10.1016/0038-092x(60)90062-1.

Li, D.H.W., Lam, T.N.T. and Chu, V.W.C., 2008b. Relationship between the total solar radiation on tilted surfaces and the sunshine hours in Hong Kong. *Solar Energy*, [online] 82(12), pp.1220–1228. https://doi.org/10.1016/j.solener.2008.06.002.

Loutzenhiser, P.G., Manz, H., Felsmann, C., Strachan, P., Frank, T. and Maxwell, G., 2007. Empirical validation of models to compute solar irradiance on inclined surfaces for building energy simulation. *Solar Energy*, [online] 81(2), pp.254–267. https://doi.org/10.1016/j.solener.2006.03.009.

Mamun, M.A.A., Hasanuzzaman, M. and Selvaraj, J., 2016. Impact of Tilt Angle on the Performance of Photovoltaic Modules in Malaysia: a

review. *4th IET Clean Energy and Technology Conference (CEAT 2016)*. [online] https://doi.org/10.1049/cp.2016.1354.

Matan, 2024. *Rayleigh scattering equation | Example of Calculation*. [online] Electricity - Magnetism. Available at: <https://www.electricity-magnetism.org/rayleigh-scattering-equation/#:~:text=The%20Rayleigh%20scattering%20equation%20quantifies,%CE%B8)%20(%CE%BB%2D4)>.

Matius, M.E., Ismail, M.A., Farm, Y.Y., Amaludin, A.E., Radzali, M.A., Fazlizan, A. and Muzammil, W.K., 2021. On the Optimal Tilt Angle and Orientation of an On-Site Solar Photovoltaic Energy Generation System for Sabah's Rural Electrification. *Sustainability*, [online] 13(10), p.5730. https://doi.org/10.3390/su13105730.

Mehleri, E.D., Zervas, P., Sarimveis, H., Palyvos, J.A. and Markatos, N.C., 2010. Determination of the optimal tilt angle and orientation for solar photovoltaic arrays. *Renewable Energy*, [online] 35(11), pp.2468–2475. https://doi.org/10.1016/j.renene.2010.03.006.

Mondragón, R., Alonso-Montesinos, J., Riveros-Rosas, D., Valdés, M., Estévez, H., González-Cabrera, A.E. and Stremme, W., 2020. Attenuation factor estimation of direct normal irradiance combining Sky camera images and mathematical models in an Inter-Tropical area. Remote Sensing, [online] 12(7), p.1212. https://doi.org/10.3390/rs12071212.

Muneer, T. and Kambezidis, H.D., 1997. *Solar radiation and daylight models for the energy efficient design of buildings*. [online] Available at: <http://ci.nii.ac.jp/ncid/BA31633435>.

Nijegorodov, N., Devan, K., Jain, P.K. and Carlsson, S., 1994. Atmospheric transmittance models and an analytical method to predict the optimum slope of an absorber plate, variously oriented at any latitude. *Renewable Energy*, [online] 4(5), pp.529–543. https://doi.org/10.1016/0960-1481(94)90215-1.

NREL, 1993. User's Manual for SERI_QC Software-Assessing the Quality of Solar Radiation Data. NREL/TP-463-5608. *Golden, CO: National Renewable Energy Laboratory*.

Ost, I., 2020. *Does solar panel temperature coefficient matter?* [online] Solar.com. Available at: <https://www.solar.com/learn/does-solar-panel-temperature-coefficient-matter/#:~:text=Most%20solar%20panels%20have%20a,decrease%20in%20efficiency%20by%200.37%25.>.

Oufettoul, H., Lamdihine, N., Motahhir, S., Lamrini, N., Abdelmoula, I.A. and Aniba, G., 2023. Comparative performance analysis of PV module positions in a solar PV array under partial shading conditions. *IEEE Access*, [online] 11, pp.12176–12194. https://doi.org/10.1109/access.2023.3237250.

Paulescu, M., Paulescu, E., Gravila, P. and Badescu, V., 2012. *Weather modeling and forecasting of PV systems operation*. Springer Science & Business Media.

Perez, R., Ineichen, P., Seals, R.K., Michalsky, J. and Stewart, R.E., 1990b. Modeling daylight availability and irradiance components from direct and global irradiance. *Solar Energy*, [online] 44(5), pp.271–289. https://doi.org/10.1016/0038-092x(90)90055-h.

Perez, R., Seals, R.K., Ineichen, P., Stewart, R.E. and Menicucci, D.F., 1987. A new simplified version of the perez diffuse irradiance model for tilted surfaces. *Solar Energy*, [online] 39(3), pp.221–231. https://doi.org/10.1016/s0038-092x(87)80031-2.

Prescott, J.A., 1940. Evaporation from a water surface in relation to solar radiation. *Transactions Royal Society South Australia*, [online] 46, pp.114–118. Available at: <https://ci.nii.ac.jp/naid/10025613338/>.

Reindl, D.T., Beckman, W.A. and Duffie, J.A., 1990. Diffuse fraction correlations. *Solar Energy*, [online] 45(1), pp.1–7. https://doi.org/10.1016/0038-092x(90)90060-p.

Reindl, D.T., Beckman, W.A. and Duffie, J.A., 1990b. Evaluation of hourly tilted surface radiation models. *Solar Energy*, [online] 45(1), pp.9–17. https://doi.org/10.1016/0038-092x(90)90061-g.

Ross, R.G., 1976. Interface design considerations for terrestrial solar cell modules. *Engineering, Environmental Science, Physics*, [online]

pp.801–806. Available at: <https://ntrs.nasa.gov/search.jsp?R=19780027121>.

Sameti, M. and Jokar, M., 2016. Numerical modelling and optimization of the finite-length overhang for passive solar space heating. *Intelligent Buildings International*, [online] 9(4), pp.204–221. https://doi.org/10.1080/17508975.2015.1134426.

Siraki, A.G. and Pillay, P., 2012. Study of optimum tilt angles for solar panels in different latitudes for urban applications. *Solar Energy*, [online] 86(6), pp.1920–1928. https://doi.org/10.1016/j.solener.2012.02.030.

Skoplaki, E., Boudouvis, A.G. and Palyvos, J.A., 2008. A simple correlation for the operating temperature of photovoltaic modules of arbitrary mounting. *Solar Energy Materials & Solar Cells/Solar Energy Materials and Solar Cells*, [online] 92(11), pp.1393–1402. https://doi.org/10.1016/j.solmat.2008.05.016.

Skeiker, K., 2009b. Optimum tilt angle and orientation for solar collectors in Syria. *Energy Conversion and Management*, [online] 50(9), pp.2439–2448. https://doi.org/10.1016/j.enconman.2009.05.031.

Tiris, M. and Tiris, C., 1998b. Optimum collector slope and model evaluation: Case study for Gebze, Turkey. *Energy Conversion and Management*, [online] 39(3–4), pp.167–172. https://doi.org/10.1016/s0196-8904(96)00229-4.

Younes, S., Claywell, R. and Muneer, T., 2005. Quality control of solar radiation data: Present status and proposed new approaches. *Energy*, [online] 30(9), pp.1533–1549. https://doi.org/10.1016/j.energy.2004.04.031.

APPENDICES

Appendix A Information on the Selected Sites for Simulation

Site Name	Latitude	Longitude	Elevation	Database		Datatype	
				SolarGis	PVGIS	TMY	TS
Marang, Terengganu, Malaysia (MY)	5.21	103.20	14	✓	✓	✓	
Ayer Keroh LSS, 77200 Bemban, Melaka, Malaysia (MY),,,,	2.29	102.34	57	✓	✓	✓	
1878, Jalan Kpb 9, Kawasan Perindustrian Balakong, 43300 Seri Kembangan, Selangor, Malaysia (MY)	3.03	101.74	53	✓		✓	
Bidor LSS, 35500 Bidor, Perak, Malaysia (MY),,,,	4.08	101.25	29	✓		✓	
1st Floor, Bintulu Airport, 97000 Bintulu, Sarawak, Malaysia (MY)	3.12	113.02	30	✓	✓	✓	
No. 3, Jalan Sungai Kayu Ara 32/39, Berjaya Industrial Park, Seksyen 32, 40460, Shah Alam, Selangor, Taman Perindustrian Berjaya, 40460 Shah Alam, Selangor, Malaysia (MY)	2.98	101.51	9	✓		✓	✓

Bukit Kayu Hitam LSS ,,,,,,,,,,,	6.48	100.43	44	✓		✓	✓
Bandar Penawar, Johor, Malaysia (MY)	1.55	104.26	36	✓		✓	
UiTM Solar Park I, Jalan Gambang, Paya Besar, 26300 Gambang, Pahang, Malaysia (MY)	3.71	103.08	67	✓	✓	✓	
Parit Raja, Johor, Malaysia (MY)	1.87	103.09	6	✓		✓	
Pendang, Kedah, Malaysia (MY)	5.86	100.54	30	✓		✓	
19, Jalan Silc 1/6, Kawasan Perindustrian Silc, 79200 Nusajaya, Johor, Malaysia (MY)	1.47	103.59	24	✓		✓	
Pasir Mas, Kelantan, Malaysia (MY)	5.99	102.11	16	✓		✓	
Lot & No: L3-08, gateway@klia2, 43900, Selangor, Malaysia (MY)	2.74	101.69	8	✓	✓	✓	
A5 Departure Gate KKIA, Sabah., 88200 Kota Kinabalu, Sabah, Malaysia (MY)	5.92	116.05	8	✓		✓	
1593, Lor 2A, Taman Sri Segedup, 93250 Kuching, Sarawak, Malaysia (MY)	1.55	110.36	6	✓	✓	✓	
Kudat, Sabah, Malaysia (MY)	6.88	116.85	8	✓	✓	✓	
Taman Intan Jaya, Mersing, Johor, Malaysia (MY)	2.45	103.81	16	✓		✓	

131, Jln Hilltop Utama 10, 98000 Miri, Sarawak, Malaysia (MY)	4.40	113.99	7	✓	✓	✓	
Penang Bayan Lepas, Malaysia (MY)	5.30	100.27	5	✓		✓	
Butterworth, Penang, Malaysia (MY)	5.43	100.44	11	✓		✓	
Axis Business Campus, Unit G.01, Block B, No.13A & 13B, Jalan 51a/225, Seksyen 51a, 46100 Petaling Jaya, Selangor, Malaysia (MY)	3.09	101.63	31	✓		✓	
Rawang, Selangor, Malaysia (MY)	3.38	101.58	64	✓		✓	
Taman Airport, Sandakan, Sabah, Malaysia (MY)	5.90	118.06	8	✓		✓	
No 3, Jalan Keluli 15/16, Seksyen 15, 40200 Shah Alam, Selangor, Malaysia (MY)	3.07	101.54	13	✓		✓	
22, Jalan Angklung 33/20, Section 33, Shah Alam Technology Park, Off Jalan Bukit Kemuning, Shah Alam, 40400, Shah Alam, Selangor, Shah Alam Technology Park, 40400 Shah Alam, Selangor, Malaysia (MY)	3.02	101.55	7	✓		✓	
Pekan Sibu, Sibu, Sarawak, Malaysia (MY)	2.29	111.80	11	✓	✓	✓	

Subang - Genting Sempah, Sultan Abdul Aziz Shah Airport (SZB), Lapangan Terbang Sultan Abdul Aziz Shah, 47200 Subang, Selangor, Malaysia (MY)	3.13	101.55	19	✓		✓	
Sungai Siput, Perak, Malaysia (MY)	4.87	101.07	107	✓		✓	
LINKWAY SHOP 2, TB15651 G FLOOR LOT 10 KUHARA POINT, LOT 10, Jalan Kuhara, 91000 Tawau, Sabah, Malaysia (MY)	4.27	117.88	22	✓		✓	
Krong Bavet, Cambodia (KH)	11.08	106.06	4	✓		✓	
FC7X+X8F Sultan Syarif Kasim II International Airport, Maharatu, Kec. Marpoyan Damai, Kota Pekanbaru, Riau 28288, Indonesia (ID)	0.47	101.45	41	✓	✓	✓	
Aua River, West Pasaman Regency, West Sumatra, Indonesia (ID)	0.10	99.55	4	✓		✓	✓
5X39+7CM Magway Airport, Magwe, Myanmar (Burma) (MM)	20.15	94.97	84	✓		✓	
PX4C+774 Mandalay International Airport, Tada-U, Myanmar (Burma) (MM)	21.71	95.97	89	✓		✓	
Cotabato City, Maguindanao, Philippines (PH)	7.23	124.21	3	✓		✓	

156 Dalongue Main Raod, Bayan ng Calasiao, Pangasinan, Philippines (PH)	16.01	120.39	8	✓		✓	
5 Engineering Drive 1, Singapore 117574 (SG)	1.30	103.77	19	✓		✓	
Yang Kram, Doi Lo District, Chiang Mai, Thailand (TH)	18.55	98.80	331	✓		✓	
Chumphon, Thailand	10.72	99.36	6	✓		✓	
21/39 à¸ªà¸™à¸²à¸¡à¸šà¸´à¸™, Tambon Aranyik, Amphoe Mueang Phitsanulok, Chang Wat Phitsanulok 65000, Thailand (TH)	16.77	100.28	44	✓		✓	
Choeng Thale, Thalang District, Phuket, Thailand (TH)	8.05	98.31	50	✓		✓	
Pak Nam Pran, Pran Buri District, Prachuap Khiri Khan, Thailand (TH)	12.34	99.98	7	✓		✓	
Thamsen, Photharam District, Ratchaburi, Thailand (TH)	13.67	99.75	62	✓		✓	
Sakom, Chana District, Songkhla, Thailand (TH)	6.95	100.80	7	✓		✓	
Makham Lom, Bang Pla Ma District, Suphan Buri, Thailand (TH)	14.41	100.08	5	✓		✓	

Khao Than, Tha Chang District, Surat Thani, Thailand (TH)	9.35	99.19	9	✓		✓	
Bo Hin, Sikao District, Trang, Thailand (TH)	7.58	99.30	24	✓		✓	
Bá°¯c BÃ¬nh District, BÃ¬nh Thuá°n Province, Vietnam (VN)	11.06	108.28	197	✓		✓	
Há°£i ChÃ¢u District, Da Nang, Vietnam (VN)	16.06	108.20	7	✓	✓	✓	

Appendix B Projection of Sunlight on Horizontal Plane (Iqbal, 1983)

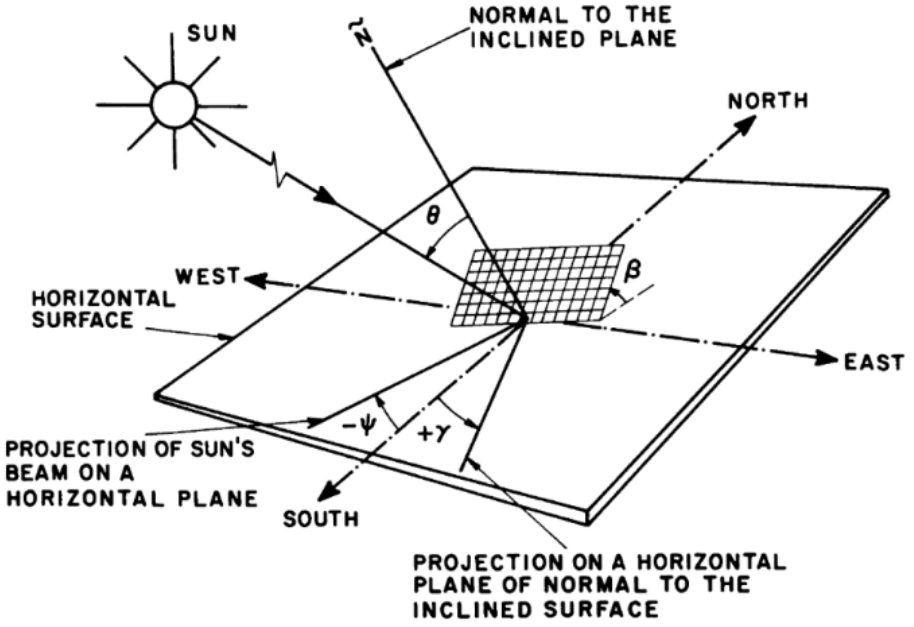

Figure 1.6.1 Position of sun relative to an inclined plane.

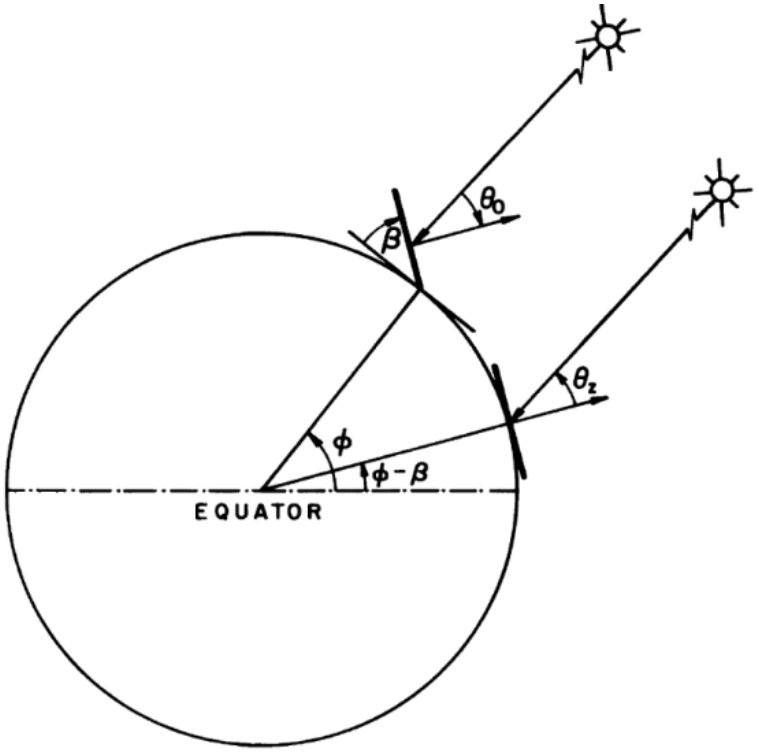

Figure 1.6.2 Diagram showing the equality of angles θ_0 and θ_z. Adapted with permission from Liu and Jordan [7].

Appendix C Work Flowchart (Chong, 2023)